Astronomy & Astrophysics manuscript no. AA19167˙v7c
March 4, 2013

Magnetic activity and differential rotation in the young Sun-like stars KIC 7985370 and KIC 7765135⋆

H.-E. Fröhlich[1], A. Frasca[2], G. Catanzaro[2], A. Bonanno[2], E. Corsaro[2,3], J. Molenda-Żakowicz[4], A. Klutsch[5], and D. Montes[5]

[1] Leibniz Institute for Astrophysics Potsdam (AIP), An der Sternwarte 16, 14482 Potsdam, Germany
[2] INAF, Osservatorio Astrofisico di Catania, via S. Sofia, 78, 95123 Catania, Italy
[3] Università di Catania, Dipartimento di Fisica e Astronomia, via S. Sofia, 78, 95123 Catania, Italy
[4] Astronomical Institute, Wrocław University, ul. Kopernika 11, 51-622 Wrocław, Poland
[5] Departamento de Astrofísica y Ciencias de la Atmósfera, Universidad Complutense de Madrid, 28040 Madrid, Spain

Received / accepted

ABSTRACT

Aims. We present a detailed study of the two Sun-like stars KIC 7985370 and KIC 7765135, aimed at determining their activity level, spot distribution, and differential rotation. Both stars were discovered by us to be young stars and were observed by the NASA *Kepler* mission.

Methods. The fundamental stellar parameters ($v \sin i$, spectral type, $T_{\rm eff}$, $\log g$, and [Fe/H]) were derived from optical spectroscopy by the comparison with both standard-star and synthetic spectra. The spectra of the targets allowed us also to study the chromospheric activity from the emission in the core of hydrogen Hα and Ca II infrared triplet (IRT) lines, revealed by the subtraction of inactive templates. The high-precision Kepler photometric data spanning over 229 days were then fitted with a robust spot model. Model selection and parameter estimation are performed in a Bayesian manner, using a Markov chain Monte Carlo method.

Results. Both stars came out to be Sun-like (G1.5 V spectral type) with an age of about 100–200 Myr, based on their lithium content and kinematics. Their youth is confirmed by the high level of chromospheric activity, which is comparable to that displayed by the early G-type stars in the Pleiades cluster. The Balmer decrement and flux ratio of the Ca II-IRT lines suggest that the formation of the core of these lines occurs mainly in optically-thick regions that are analogous to solar plages. The spot model applied to the *Kepler* photometry requires at least seven enduring spots in the case of KIC 7985370 and nine spots in the case of KIC 7765135 for a satisfactory fit of the data. The assumption of longevity of the star spots, whose area is allowed to evolve in time, is at the heart of our spot-modelling approach. On both stars the surface differential rotation is Sun-like, with the high-latitude spots rotating slower than the low-latitude ones. We found, for both stars, a rather high value of the equator-to-pole differential rotation ($d\Omega \approx 0.18$ rad d^{-1}) which is in contrast with the predictions of some mean-field models of differential rotation for fast-rotating stars. Our results are instead in agreement with previous works on solar-type stars and with other models which predict a higher latitudinal shear, increasing with equatorial angular velocity, that can undergo changes along the magnetic cycle.

Key words. Stars: activity – stars: starspots – stars: rotation – stars: chromospheres – stars: individual: KIC 7985370 and KIC 7765135 – X-rays: stars

1. Introduction

In the Sun, magnetic activity is thought to be produced by a global-scale dynamo action arising from the coupling of convection and rotation (Parker 1955; Steenbeck et al. 1966). Young Sun-like stars are rotating faster than the Sun and display a much higher level of magnetic activity at all atmospheric layers, which is likely due to a stronger dynamo action. They also show different manifestations of activity compared to the Sun, such as bigger and long-living spots in their photospheres, active longitude belts, absence or a different behaviour of activity cycles, highly energetic flares, etc. These differences are likely related to the dynamo mechanism, which is operating in rather different conditions in young stars mainly regarding their rotation rate and internal structure. Understanding the properties of young suns and, particularly, their activity and rotation, is crucial to trace the Sun and its environment back to the first evolutionary stages.

In fact the properties of the magnetoconvection in these stars seems to be strongly influenced by the Ω-effect that produces characteristic "wreaths" on large scales (Nelson et al. 2011). Although strong latitudinal variations of the differential rotation can be obtained by means of the combined role of thermal wind balance and geostrophy, the results of numerical simulations seem to be strongly dependent on the Reynolds number of the flow. The situation is at variance with the dynamo action in main sequence solar-type stars, where the role of the tachocline is instead essential in producing the α effect (Dikpati & Gilman 2001; Bonanno et al. 2002; Bonanno 2012).

It is still unclear whether a strong latitudinal differential rotation is common among fast-rotating stars. Marsden et al. (2011) report values of the absolute differential rotation dΩ in the range

Send offprint requests to: H.-E. Fröhlich
e-mail: hefroehlich@aip.de

⋆ Based on public *Kepler* data, on observations made with the Italian Telescopio Nazionale Galileo (TNG) operated by the Fundación Galileo Galilei – INAF at the Observatorio del Roque del los Muchachos, La Palma (Canary Islands), on observations collected at the 2.2-m telescope of the Centro Astronómico Hispano Alemán (CAHA) at Calar Alto (Almería, Spain), operated jointly by the Max-Planck-Institut für Astronomie and the Instituto de Astrofísica de Andalucía (CSIC), and on observations collected at the Catania Astrophysical Observatory (Italy).

0.08–0.45 rad d^{-1} for a sample of rapid rotators similar to and slightly more massive than the Sun. Despite the spread of values, it seems that dΩ is in any case larger than in the Sun. The measures of absolute differential rotation in a large sample of F- and early G-type stars through the Fourier transform technique (Reiners & Schmitt 2003; Reiners 2006) show no indication of the decrease in this parameter with the rotation period, rather the highest values of dΩ are encountered for periods between 2 and 3 days. On the other hand, some recent calculations predict a moderate differential rotation, comparable to that of the Sun, also for a Sun-like star rotating 20 times faster (e.g., Küker et al. 2011).

Moreover, dΩ seems also to be a function of the stellar mass for main-sequence stars, increasing with their effective temperature, as shown, e.g., by Barnes et al. (2005). One of the largest values of differential rotation for a star noticeably cooler than the Sun was found by us (Frasca et al. 2011, hereafter Paper I) for KIC 8429280, a 50 Myr-old K2-type star, from the analysis of the light curve collected by the NASA *Kepler* spacecraft.

The highly precise photometry of *Kepler* (Borucki et al. 2010; Koch et al. 2010) coupled with the long and virtually uninterrupted coverage makes these data unique for the study of photospheric activity and differential rotation in late-type stars, as we have shown in our first work based on the analysis of *Kepler* data of spotted stars (Paper I).

However, whether star spots are indeed the best tracers of the surface rotation or not is still a matter of debate (for a different point of view, see Korhonen & Elstner 2011).

As for KIC 8429280 (Paper I), the two new targets KIC 7985370 (HD 189210 = 2MASS J19565974+4345083 = TYC 3149-1571-1) and KIC 7765135 (2MASS J19425057 +4324486 = TYC 3148-2163-1) were selected as active stars from their optical variability and from the cross-correlation of the ROSAT All-Sky Survey (RASS; Voges et al. 1999, 2000) with Tycho and Hipparcos catalogues (Perryman et al. 1997). With $V = 10\overset{\mathrm{m}}{.}0$ and $11\overset{\mathrm{m}}{.}8$, respectively, both stars are relatively bright ones in the *Kepler* field of view. Both of them were recently reported as variable by Pigulski et al. (2009), who searched for bright variable stars in the *Kepler* field of view with ASAS3-North station. The variability of KIC 7985370 could be due to a rotational modulation according to Uytterhoeven et al. (2011) that rely on the first two quarters of *Kepler* data. The *Kepler* light curves readily show these stars as rotationally variable with a period of about 2–3 days, which is typical of G-type stars in the Pleiades cluster (age ≈ 130 Myr, Barrado y Navascués et al. 2004). The estimates of their atmospheric parameters reported in the *Kepler* Input Catalog (KIC), which are based on Sloan photometry (for a revised temperature scale cf. Pinsonneault et al. 2012), suggested to us that these objects were similar to the Sun.

The analysis of the optical spectra collected by us confirmed that the stars are nearly identical to the Sun, but much younger and as such deserving a detailed investigation. Applying the same techniques as in Paper I, we determined the basic stellar parameters (Sect. 3.1), the chromospheric activity (Sect. 3.2), and elements abundances (Sect. 3.3). The kinematics of these stars is shortly discussed in Sect. 3.5. The Bayesian approach to spot modelling applied to the *Kepler* light curves is described in Sect. 4 and the results are presented and discussed in Sect. 5 with particular relevance to the issue of differential rotation.

2. Ground-based observations and data reduction

2.1. Spectroscopy

Two spectra of KIC 7985370 with a signal-to-noise ratio S/N of about 60–70 were collected at the *M. G. Fracastoro* station (Serra La Nave, Mt. Etna, 1750 m a.s.l.) of the *Osservatorio Astrofisico di Catania* (OAC, Italy) in July and October 2009. The 91-cm telescope of the OAC was equipped with FRESCO, a fiber-fed *échelle* spectrograph that, with the 300-lines/mm cross-disperser, covers the spectral range 4300–6800 Å with a resolution $R = \lambda/\Delta\lambda \approx 21\,000$.

Another spectrum of KIC 7985370 with S/N≈ 120 was taken with SARG, the *échelle* spectrograph at the Italian *Telescopio Nazionale Galileo* (TNG, La Palma, Spain) on 2009 August 12 with the red grism and the slit width of $0\overset{''}{.}8$. This spectrum, covering the 5500–11 000 Å wavelength range, has a resolution $R \approx 57\,000$.

The spectrum of KIC 7765135 was taken on 2009 October 3 with the Fiber Optics Cassegrain *Échelle* Spectrograph (FOCES; Pfeiffer et al. 1998) at the 2.2-m telescope of the Calar Alto Astronomical Observatory (CAHA, Almería, Spain). The 2048×2048 CCD detector Site#1d (pixel size = 24 μm) and the slit width of 400 μm give rise to a resolution $R \approx 28\,000$ and a S/N≈ 100 in the red wavelength region with a 30-minutes exposure time.

Spectra of radial (RV) and rotational velocity ($v \sin i$) standard stars (Table 1), as well as bias, flat-field, and arc-lamp exposures were acquired during each observing run and were used for the data reduction and analysis.

The data reduction was performed with the ECHELLE task of the IRAF[1] package (see, e.g., Frasca et al. 2010; Catanzaro et al. 2010, for details).

Table 1. Radial/rotational velocity standard stars.

Name	Sp. Type	*RV* (km s^{-1})	$v \sin i^c$ (km s^{-1})	Notes[d]
HD 10307	G1.5 V	4.0[b] *	2.1	$v \sin i$
HD 10700	G8 V	−17.1[b]	0.9	$v \sin i$
HD 157214	G0 V	−79.2[b]	1.6	$v \sin i$
HD 182572	G8 IV	−100.35[a]	1.9	*RV*, $v \sin i$
HD 187691	F8 V	0.0[a]	2.8	*RV*

Notes. [(a)] Udry et al. (1999). [(b)] Nordström et al. (2004). [(c)] Glebocki & Gnacinski (2005). [(d)] *RV* = radial velocity standard star; $v \sin i$ = standard for rotational velocity. [(*)] Variable?

2.2. Photometry

The focal-reducer CCD camera at the 91-cm telescope of OAC was used, on 2009 December 10, to perform standard photometry in the Johnson-Cousins B, V, R_C, and I_C bands. The data were reduced following standard steps of overscan region subtraction, master-bias subtraction, and division by average twilight flat-field images. The BVR_CI_C magnitudes were extracted from the corrected images through aperture photometry performed with

[1] IRAF is distributed by the National Optical Astronomy Observatory, which is operated by the Association of the Universities for Research in Astronomy, inc. (AURA) under cooperative agreement with the National Science Foundation.

Table 2. Stellar parameters. The data of the upper part is from the literature.

		KIC 7985370	KIC 7765135
RA	(J2000)	$19^h56^m59^s.74$	$19^h42^m50^s.58$
DEC	(J2000)	$+43°45'08''.3$	$+43°24'48''.7$
X-ray count[a]	[ct/s]	0.033 ± 0.008	...
J[b]		8.789 ± 0.020	10.414 ± 0.025
H[b]		8.507 ± 0.063	10.113 ± 0.020
K_s[b]		8.419 ± 0.033	10.028 ± 0.014
B		10.59 ± 0.09	12.50 ± 0.09
V		9.98 ± 0.08	11.82 ± 0.08
R_C		9.57 ± 0.06	11.28 ± 0.06
I_C		9.33 ± 0.06	10.97 ± 0.06
Sp. Type		G1.5 V	G1.5 V
T_{eff}	[K]	5815 ± 95	5835 ± 95
$\log g$		4.24 ± 0.12	4.34 ± 0.12
[Fe/H]		−0.05 ± 0.10	0.04 ± 0.05
$v \sin i$[c]	[km s^{-1}]	18.2 ± 1.3	21.4 ± 1.1
$v \sin i$[d]	[km s^{-1}]	17.9 ± 1.3	21.9 ± 1.3
RV	[km s^{-1}]	−24.0 ± 0.3	−20.0 ± 0.2
W(Li)	[mÅ]	155 ± 20	160 ± 20
$\log N$(Li)[e]		2.87 ± 0.10	2.93 ± 0.10
Age	[Myr]	100 – 200	100 – 200
Mass	[$M_\odot$]	1.15 ± 0.10	1.15 ± 0.10
Distance	[pc]	113 ± 15	245 ± 30
U	[km s^{-1}]	−8.63 ± 0.86	−5.61 ± 1.73
V	[km s^{-1}]	−22.03 ± 0.37	−18.14 ± 0.57
W	[km s^{-1}]	−6.74 ± 0.84	−7.86 ± 1.93

Notes. [(a)] From the ROSAT All-Sky Survey Faint Source Catalogue (Voges et al. 2000). [(b)] JHK_s magnitudes are from 2MASS catalogue (Cutri et al. 2003). [(c)] From ROTFIT code. [(d)] From $FWHM$–$v \sin i$ calibration. [(e)] Calculated by means of a spectral synthesis based on ATLAS9 atmospheric models (Sect. 3.3).

DAOPHOT by using the IDL[2] routine APER. Standard stars in the cluster NGC 7790 and in the field of BL Lac (Stetson 2000) were used to calculate the zero points and the transformation coefficients to the Johnson-Cousins system. Photometric data derived in this work and JHK_s magnitudes from 2MASS (Cutri et al. 2003) are summarized in Table 2.

3. Target characterization from ground-based observations

3.1. Astrophysical parameters

The analysis of the high-resolution spectra was aimed at measuring the radial (RV) and projected rotational velocities ($v \sin i$), performing the MK spectral classification, and deriving basic stellar parameters like effective temperature (T_{eff}), gravity ($\log g$), and metallicity ([Fe/H]).

We have computed the cross-correlation functions (CCFs) with the IRAF task FXCOR adopting spectra of late-F and G-type slowly-rotating stars (Table 1), which were acquired with the same setups and during the same observing nights as our targets. The latter were used both for the measure of RV and the determination of $v \sin i$ through a calibration of the full-width at half maximum ($FWHM$) of the CCF peak as a function of the $v \sin i$ of their artificially broadened spectra (see, e.g., Guillout et al. 2009; Martínez-Arnáiz et al. 2010). We averaged the results from individual *échelle* orders as described, e.g., in Frasca et al. (2010) to get the final RV and $v \sin i$ of our young Sun-like stars.

For KIC 7985370, we measured, within the errors, the same RV in the FRESCO spectra taken on 2009 July 10 ($RV = -23.9 \pm 0.4$ km s^{-1}) and on 2009 October 4 ($RV = -24.2 \pm 0.4$ km s^{-1}), while a value of $RV = -21.8 \pm 0.2$ km s^{-1} has been derived from the SARG spectrum of 2009 August 12. This could indicate a true RV variation just above the 3-σ confidence level. However, much more spectra are needed to prove or disprove such a RV variation and to make sure that the star is a single-lined spectroscopic binary.

For KIC 7765135, we only acquired one spectrum from which we derived an RV of -20.0 ± 0.2 km s^{-1}.

Since we found no indication for binarity (visual or spectroscopic) in the literature for both stars, we consider them as being single stars or, at most, single-lined spectroscopic binaries for which the eventual companions are too faint to give a significant contribution neither to the optical spectrum nor to the *Kepler* photometry.

For the SARG spectrum, we used the ROTFIT code (Frasca et al. 2003, 2006) to evaluate T_{eff}, $\log g$, [Fe/H], and redetermine $v \sin i$, adopting a library of ELODIE Archive spectra of standard stars, as described in Paper I. To match the lower resolution ($R_{FOCES} = 28\,000$) of the FOCES spectrum, the ELODIE templates ($R_{ELODIE} = 42\,000$) were convolved with a Gaussian kernel of $FWHM = \lambda \sqrt{1/R^2_{FOCES} - 1/R^2_{ELODIE}}$ Å before running ROTFIT. We applied the ROTFIT code only to the *échelle* orders with a fairly good S/N, which span the ranges 5600–6700 Å and 4300–6800 Å for SARG and FOCES spectra, respectively. The spectral regions heavily affected by telluric lines were excluded from the analysis. The adopted estimates for the stellar parameters and the associated uncertainties come from a weighted mean of the values derived for all the individual orders, as described in Paper I. We also applied this procedure to the FRESCO spectra of KIC 7985370, obtaining stellar parameters in very close agreement with those derived from the SARG spectrum.

ROTFIT also allowed us to measure $v \sin i$ by matching to the observed spectrum the spectra of slowly-rotating standard stars artificially broadened at an increasing $v \sin i$ and finding the minimum of χ^2. For this purpose, we used the standard stars listed in Table 1 because their spectra were acquired with the same instrumental setup as that used for our targets, avoiding the introduction of any systematic error caused by a different resolution.

We obtained nearly the same values of the astrophysical parameters for both targets. They turn out to be very similar to the Sun, both in spectral type and effective temperature, but considerably younger, as testified by the high lithium content in their photospheres (Sect. 3.3). Their average values and standard errors are reported in Table 2.

Based on these parameters and the age estimate (Sects. 3.3 and 3.5), compatible with zero-age main-sequence (ZAMS) stars, we can roughly estimate their mass and radius as $M = 1.15 \pm 0.10\, M_\odot$ and $R = 1.1 \pm 0.1\, R_\odot$ from evolutionary tracks (e.g., Siess et al. 2000).

3.2. Chromospheric activity

The high level of magnetic activity in the chromosphere is displayed by the Ca II IRT and Hα lines that are strongly filled-in by emission (Figs. 1 and 2). The He I D_3 (λ 5876Å) absorption line is clearly visible in the spectra of our two young suns (Figs. 1 and

[2] IDL (Interactive Data Language) is a registered trademark of ITT Visual Information Solutions.

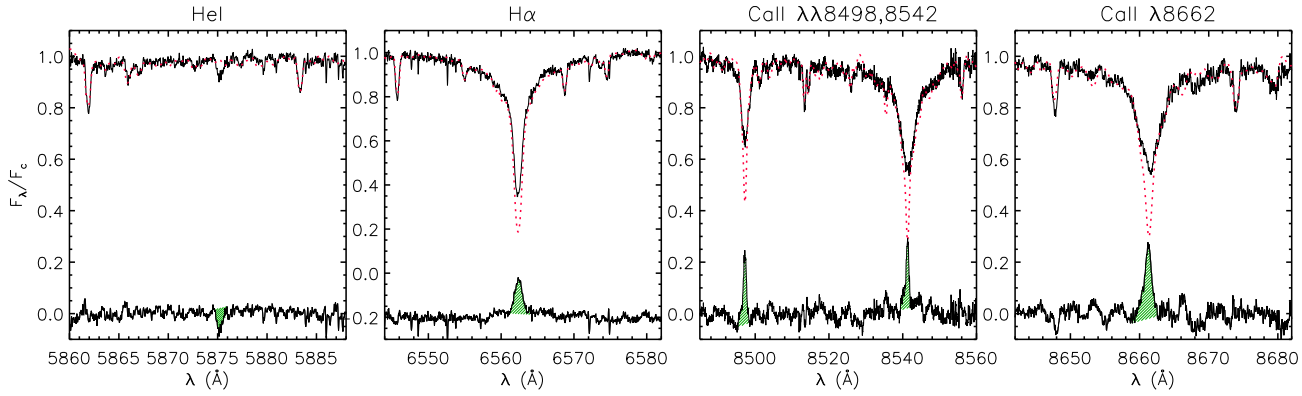

Fig. 1. *Top of each panel*: Observed, continuum-normalized SARG spectrum of KIC 7985370 (solid line) in the He I D_3, Hα, and Ca II IRT regions together with the non-active stellar template (dotted red line). *Bottom of each panel*: Difference between observed and template spectra. The residual Hα profile is plotted shifted downwards by 0.2 for the sake of clarity. The hatched areas represent the excess emissions (absorption for He I) that have been integrated to get the net equivalent widths.

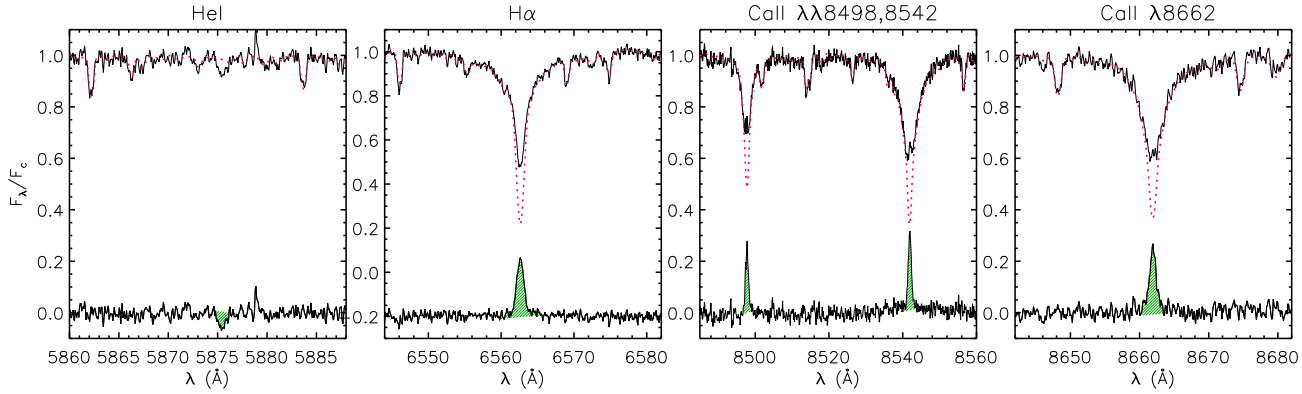

Fig. 2. As Fig. 1, but for the FOCES spectrum of KIC 7765135.

2). This implies the presence of an upper chromosphere because a temperature of at least 10 000 K is required for its formation.

We estimated the chromospheric emission level with the "spectral subtraction" technique (see, e.g., Frasca & Catalano 1994; Montes et al. 1995). This procedure is based on the subtraction of a reference "non-active" template made with observed spectra of slowly-rotating stars of the same spectral type as the investigated active stars, but with a negligible level of chromospheric activity and an undetectable lithium line. The equivalent width of the lithium and helium absorption lines ($W_{\rm Li}$ and $W_{\rm He}$, respectively) and the net equivalent width ($W^{\rm em}$) of the Ca II IRT and Hα lines were measured from the spectrum obtained after subtracting the non-active template from the target and then by integrating the residual emission (absorption for the lithium and helium lines) profile, which is represented by the hatched areas in Figs. 1 and 2.

We noted a significant variation of the Hα emission in the three spectra of KIC 7985370, with $W^{\rm em}_{\rm H\alpha}$ ranging from 160 to 264 mÅ (Table 3).

The radiative losses in the chromospheric lines were evaluated by multiplying the average $W^{\rm em}$ by the continuum surface flux at the wavelength of the line, in the same way as in Frasca et al. (2010). The net equivalent widths and the chromospheric fluxes are reported in Table 3.

The Hβ net equivalent width could be measured only for KIC 7765135 because the SARG spectrum of KIC 7985370 does not include that wavelength region. In the FRESCO spectra, it is not possible to apply the subtraction technique, due to the very low S/N ratio in that spectral region, which prevented us from detecting such a tiny filling of the line.

For KIC 7765135 we measured a Balmer decrement $F_{\rm H\alpha}/F_{\rm H\beta} = 4.3 \pm 2.5$ that is slightly larger than the values in the range 2–3 found by us for KIC 8429280 (Paper I) and for HD 171488 (Frasca et al. 2010). Accounting for the error, this ratio is however still compatible with optically-thick emission by atmospheric features similar to solar and stellar plages (e.g., Buzasi 1989; Chester 1991) rather than to prominence-like structures, for which a Balmer decrement of the order of 10 is expected (e.g., Landman & Mongillo 1979; Hall & Ramsey 1992).

The Ca II-IRT flux ratio, $F_{8542}/F_{8498} = 1.4 \pm 0.9$, is indicative of high optical depths and is in the range of the values found by Chester (1991) in solar plages. The optically-thin emission from solar prominences gives rise instead to values of $F_{8542}/F_{8498} \sim 9$. We measured a value of $F_{8542}/F_{8498} = 1.6 \pm 1.0$ for KIC 7985370, that is almost the same as KIC 7765135.

The chromospheric emission in both stars appears thus to be mainly due to surface regions similar to solar plages, while the quiet chromosphere and eventual prominences play a marginal role.

The subtraction technique also allowed us to measure the lithium equivalent width cleaned up from the contamination

Table 3. Line equivalent widths and chromospheric fluxes.

Line	Date (yyyy/mm/dd)	UT_{mid} (hh:mm)	W^{em} (mÅ)	Error (mÅ)	Flux (erg cm^{-2} s^{-1})
		KIC 7985370			
Hα	2009/07/10	22:29	160	40	1.23×10^6
”	2009/08/12	04:18	264	30	2.02×10^6
”	2009/10/03	19:17	202	35	1.55×10^6
He I D_3	2009/08/12	04:18	-50^a	20	...
Ca II λ8498	” ”	” ”	263	55	1.33×10^6
Ca II λ8542	” ”	” ”	439	55	2.16×10^6
Ca II λ8662	” ”	” ”	337	60	1.66×10^6
		KIC 7765135			
Hα	2009/10/03	20:15	326	60	2.48×10^6
Hβ	” ”	” ”	54	30	0.58×10^6
He I D_3	” ”	” ”	-60^a	25	...
Ca II λ8498	” ”	” ”	258	45	1.28×10^6
Ca II λ8542	” ”	” ”	366	45	1.76×10^6
Ca II λ8662	” ”	” ”	328	65	1.58×10^6

Notes. [(a)] The minus sign for the W^{em} indicates a residual absorption (He I line).

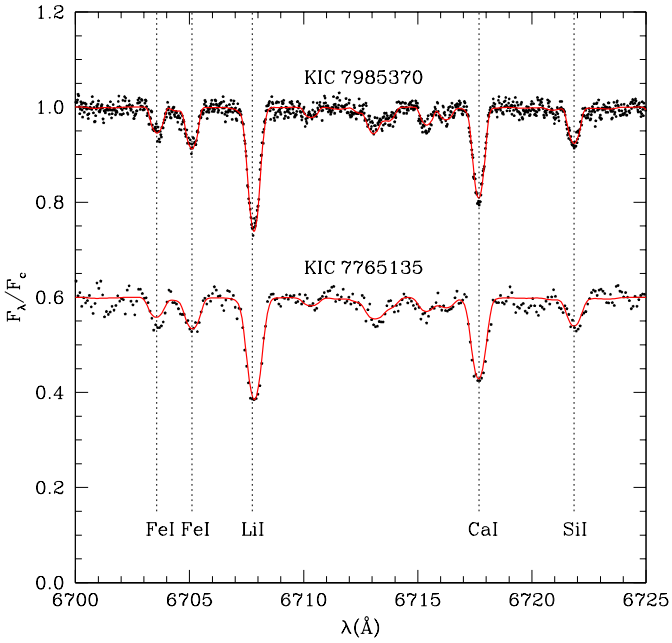

Fig. 3. Observed spectra (dots) of KIC 7985370 and KIC 7765135 (shifted downwards by 0.4) in the Li I λ6707.8 Å region together with the synthetic spectra (full lines).

of Fe I λ6707.4 Å line, which is strongly blended with the nearby Li I line (Fig. 3). The lithium equivalent width measured for KIC 7985370 (W_{Li} = 155 ± 20 mÅ) and for KIC 7765135 (W_{Li} = 160 ± 20 mÅ), just above the Pleiades upper envelope (Soderblom et al. 1993a), translates into a very high lithium abundance, log N(Li) = 3.0 ± 0.1, for both stars, as results from the calibrations of Pavlenko & Magazzù (1996). The determination of lithium abundance was refined in Sect. 3.3 by means of a spectral synthesis based on ATLAS9 atmospheric models (Kurucz 1993).

3.3. Abundance analysis

Since the spectral features in our two stars are relatively broad, it is difficult to find unblended lines for measuring their equivalent widths. To overcome this problem, the photospheric abundances were thus estimated by matching a rotationally-broadened synthetic spectrum to the observed one. For this purpose, we divided each spectrum into 50 Å-wide segments, which were analyzed separately. The spectral ranges 4450–8650 Å and 5600–7300 Å were used for the spectra of KIC 7765135 and KIC 7985370, respectively. The synthetic line profiles were computed with SYNTHE (Kurucz & Avrett 1981) using ATLAS9 (Kurucz 1993) atmospheric models. All models were calculated using the solar opacity distribution function and a microturbulence velocity $\xi = 2$ km s^{-1}. For each segment, the abundance was determined by χ^2 minimization. We used the spectral line list and atomic parameters from Castelli & Hubrig (2004) that are updated from Kurucz & Bell (1995).

The error in the abundance of one particular element was taken as the standard deviation of the mean of the abundances calculated for each segment. For elements whose lines occurred in only one or two segments, the error in the abundance was evaluated by varying the effective temperature and gravity within their uncertainties (as given in Table 2) and computing the abundance for T_{eff} and log g values within these ranges. We found a variation of ≈ 0.1 dex in abundance due to temperature variation, but no significant variation when log g was varied. Thus the uncertainty in temperature is probably the main source of error in the abundance estimation. In Fig. 3 we show an example of the matching between synthetic and observed spectra. To determine the Li abundance, we used the Li I λ6707 Å line, taking into account the hyperfine structure (Andersen et al. 1984). The abundances are given in Table 4.

Fig. 4 shows a comparison between the abundances derived for our targets and the solar values from Grevesse et al. (2010). With the exception of lithium, all the other abundances are rather similar to those measured for the solar photosphere. In particular, we note that KIC 7765135 is ≈ 0.3 dex more metallic than the Sun, which confirms the results of ROTFIT (Table 2).

As far as the lithium is concerned, we converted the abundance from log N/N_{tot} to log N/N(H) on a scale where log N(H) = 12, finding log N(Li) = 2.93 ± 0.10 and 2.87 ± 0.10 for KIC 7765135 and KIC 7985370, respectively. These values are smaller than, but marginally consistent with, those obtained from the equivalent widths and the calibrations of Pavlenko & Magazzù (1996) and reported in Sect. 3.2.

For early G-type stars, like our targets, the lithium abundance does not give a very strong constraint on their age. Indeed, their log N(Li) remains close to the initial lithium abundance for Population I stars (log N(Li)=3.1–3.3) during their early life. It has been shown that stars with temperatures in the range T_{eff} = 5900 ± 150 K display a significant lithium depletion (log N(Li) = 2.9) only after about 150 Myr (see, e.g., Sestito & Randich 2005). Thus, we can estimate an age of the order of 100–200 Myr for both stars with a lower limit of roughly 30–50 Myr, being the lithium abundance below the upper envelope of the α Per (age ≈ 50 Myr) and IC 2602 (age ≈ 30 Myr) clusters (Montes et al. 2001b; Sestito & Randich 2005). Moreover, the absence of a strong near-IR excess in their spectral energy distributions (see Sect. 3.4) and of accretion signatures in the spectrum, allows us to exclude an age of a few million years for both stars that should already be in a post-T Tauri phase (age ≥ 10–20 Myr).

Table 4. Abundances inferred for our two stars expressed in the form $\log N/N_{\rm tot}$.

Elem.	KIC 7985370	KIC 7765135
Li	−9.10 ± 0.10	−9.04 ± 0.10
C	−3.67 ± 0.10	−3.29 ± 0.14
O	...	−3.10 ± 0.10
Na	−5.77 ± 0.16	−5.68 ± 0.12
Mg	−4.67 ± 0.11	−4.77 ± 0.13
Al	−5.48 ± 0.17	−5.64 ± 0.19
Si	−4.51 ± 0.17	−4.48 ± 0.14
Ca	−5.70 ± 0.09	−5.42 ± 0.14
Ti	−7.12 ± 0.16	−6.88 ± 0.15
V	−8.00 ± 0.16	−7.87 ± 0.14
Cr	−6.20 ± 0.16	−6.40 ± 0.10
Mn	−6.74 ± 0.20	−6.52 ± 0.17
Fe	−4.68 ± 0.18	−4.65 ± 0.11
Co	−6.95 ± 0.13	−6.82 ± 0.09
Ni	−5.94 ± 0.12	−5.92 ± 0.12
Cu	−8.11 ± 0.06	−8.13 ± 0.17
Ba	−10.28 ± 0.12	−10.11 ± 0.15

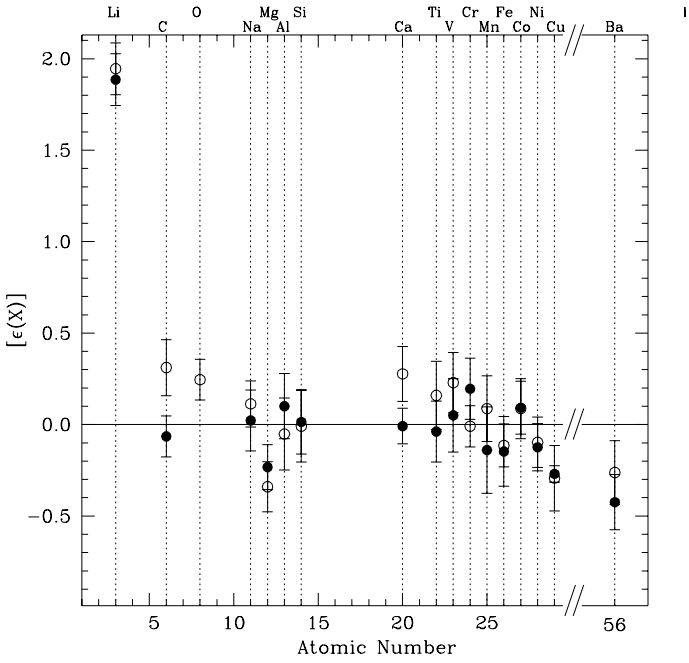

Fig. 4. Abundances found for KIC 7765135 (open circles) and for KIC 7985370 (filled circles) related to the solar ones.

3.4. Spectral energy distributions

The spectral energy distributions (SEDs) from the optical to the near-infrared (IR) domain were obtained by merging our standard $UBVR_{\rm C}I_{\rm C}$ photometry (Table 2) with JHK_s magnitudes from the 2MASS catalogue (Cutri et al. 2003).

We used the grid of NextGen low-resolution synthetic spectra, with $\log g = 4.0$ and 4.5 and solar metallicity by Hauschildt et al. (1999), to perform a fit to the SEDs. The effective temperature ($T_{\rm eff}$) was kept fixed to the value derived with ROTFIT (Table 2) for each target. The interstellar extinction (A_V) was evaluated from the distance according to the rate of 0.8 mag/kpc found by Mikolajewska & Mikolajewski (1980) for the sky region around CI Cyg (very close to our targets). The Cardelli et al. (1989) extinction law with $R_V = 3.1$ was used for

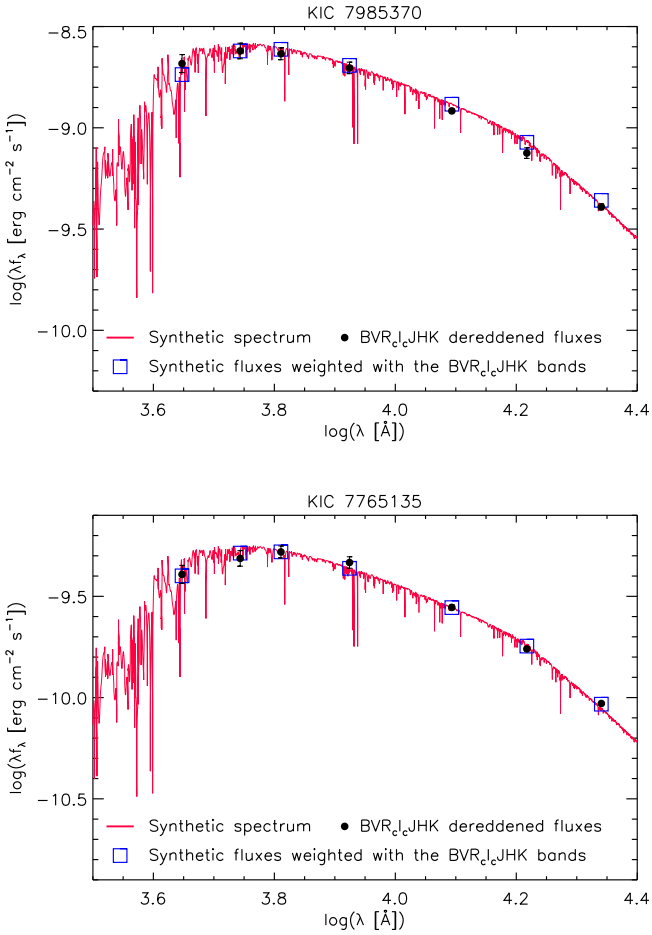

Fig. 5. Spectral energy distributions (dots) for KIC 7985370 *(top panel)* and KIC 7765135 *(bottom panel)*. The NextGen synthetic spectrum at $T_{\rm eff} = 5800$ K scaled to the star distance is overplotted with continuous lines in each box.

evaluating the extinction in the other bands. Finally, the angular diameter (ϕ) that scales the synthetic surface flux over the stellar flux at Earth, was left free to vary. The best solution was found by minimizing the χ^2 of the fit to the $BVR_{\rm C}I_{\rm C}J$ data, which are dominated by the photospheric flux of the star and are normally not significantly affected by infrared excesses. The angular diameter derived for KIC 7985370, $\phi = 0.0895$ mas, implies a distance $d = 113 \pm 15$ pc, if we adopt a ZAMS radius of 1.1 $R_\odot$ (Sect. 3.1). For KIC 7765135 we found $\phi = 0.0413$ mas, which corresponds to $d = 245 \pm 30$ pc, adopting again 1.1 $R_\odot$. The error in the distance is estimated taking into account both a 0.1-$R_\odot$ uncertainty in the stellar radius and the temperature error of about 100 K (see Table 2).

As apparent in Fig. 5, the SEDs are well reproduced by the synthetic spectrum till the K_s band both for KIC 7985370 and KIC 7765135 and no excess is visible at near-IR wavelengths. This strengthens the spectroscopic determination of the effective temperature and ensures that these stars have by far gone over the T Tauri phase, during which a thick and dense accretion disk gives rise to a conspicuous infrared excess. The absence of mid- and far-infrared data does not allow us to exclude the presence of thinner "debris" disks, like those found in a few Pleiades solar-type stars (Stauffer et al. 2005; Gorlova et al. 2006).

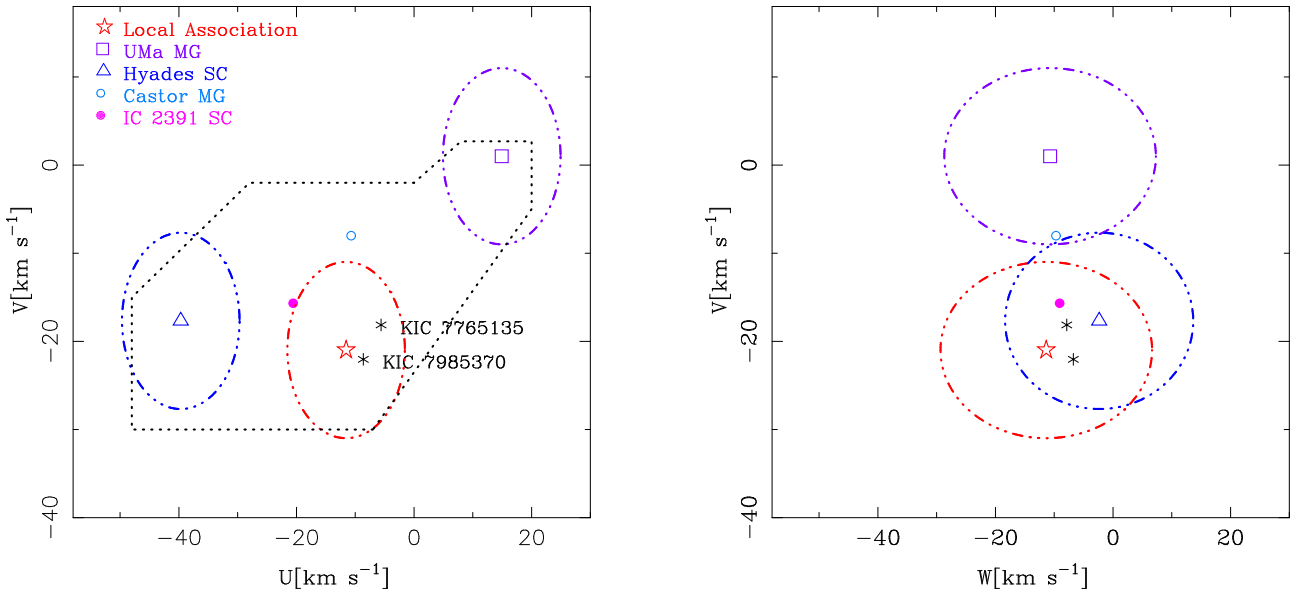

Fig. 6. (U, V) and (W, V) planes of our two young suns. We plotted the average position of each young stellar kinematic group with different symbols. The dotted line in the left panel demarcates the locus of the young-disk population (age < 2 Gyr) in the solar neighborhood, as defined by Eggen (1984, 1989).

3.5. Kinematics

We used the radial velocities determined in Sect. 3.1 and the distances estimated in Sect. 3.4 together with measurements of proper motions taken from the Tycho-2 catalogue (Høg et al. 2000), to calculate Galactic space-velocity components (U, V, W), following the procedures described in Montes et al. (2001a). The values, listed in Table 2, are given in a right-handed coordinate system (positive toward the Galactic anti-center, in the Galactic rotation direction, and toward the north Galactic pole, respectively). In the (U, V) and (W, V) Bottlinger diagrams (Fig. 6), we have plotted the locus of our targets. Different symbols represent the central position given in the literature (see Montes et al. 2001a) of the five youngest and best documented moving groups (MGs) and superclusters (SCs): namely the Local Association (LA) or Pleiades MG (20–150 Myr), the IC 2391 SC (35–55 Myr), the Castor MG (200 Myr), the Ursa Major (UMa) MG or Sirius supercluster (300 Myr), and the Hyades SC (600 Myr).

The space velocities of these two Sun-like stars are consistent with those of the young-disk population (Fig. 6). Based on two different statistical methods (for further information, see Klutsch et al. (2010) and the paper in preparation by Klutsch et al. (2012), we determined their membership probability to each of the five aforementioned young stellar kinematic groups. KIC 7985370 and KIC 7765135 fall in the Local Association (LA) locus. With a probability of more than 70 %, they turn out to be highly likely members of this moving group. Furthermore, such a result is absolutely in agreement with the age derived from the lithium abundance (Sect. 3.3).

4. Spot modelling of the Kepler light curves

4.1. Photometric data

All the available public *Kepler* long-cadence time-series ($\Delta t \approx$ 30 min, Jenkins et al. 2010), spanning from 2009 May 2 to 2009 December 16, was analyzed. It covers altogether 229 days and corresponds to the observing quarters 0–3 (Q0–Q3), with the largest gap, about 4.5 days, appearing between Q1 and Q2.

To remove systematic trends in the *Kepler* light curves associated with the spacecraft, detector, and environment, and to prepare them for the analysis of star spots that we will describe below, we used the software KEPCOTREND[3]. This procedure is based on Cotrending Basis Vectors (CBV), which are calculated (and ranked) through singular value decomposition and describe the systematic trends present in the ensemble flux data for each CCD channel. We used the first two basis vectors for Q0 data, while from three to five CBV were adopted for the correction of longer data sets such as Q1, Q2, and Q3.

In order to check how the data rectification accomplished with KEPCOTREND is reflected in the outcome, the spot modelling has been done twice: with the rectified data (Case A) as well as with the original data (Case B).

The power spectra of the *Kepler* time-series, cleaned by the spectral window according to Roberts et al. (1987), are displayed in Fig. 7. The lower panel of Fig. 7 clearly shows two main peaks for KIC 7765135, which are close in frequency (0.391 and 0.414 d^{-1}). The corresponding periods are 2.560±0.015 and 2.407±0.014 days, respectively. The period errors are from the *FWHM* of the spectral window. The low-amplitude peaks at frequency of ≈ 0.8 d^{-1} are overtones of the two main peaks. As visible from the upper panel of Fig. 7, the structure of the peaks for KIC 7985370 is more complex, with the maximum corresponding to 2.856±0.019 days and a second peak, blended with the first one on its low-frequency side, at 2.944 days. A third small peak corresponding to P = 3.090 days is also visible.

Such a double- or multiple-peaked periodogram hints at differential rotation. As Lanza et al. (1994) predicted, a photometric time series, if sufficiently accurate ($\Delta F/F = 10^{-5} - 10^{-6}$), may reveal a Sun-like latitudinal differential rotation.

An estimate of the inclination of the rotation axis with respect to the line of sight is very useful to constrain the spot

[3] http://keplergo.arc.nasa.gov/ContributedSoftwareKepcotrend.shtml

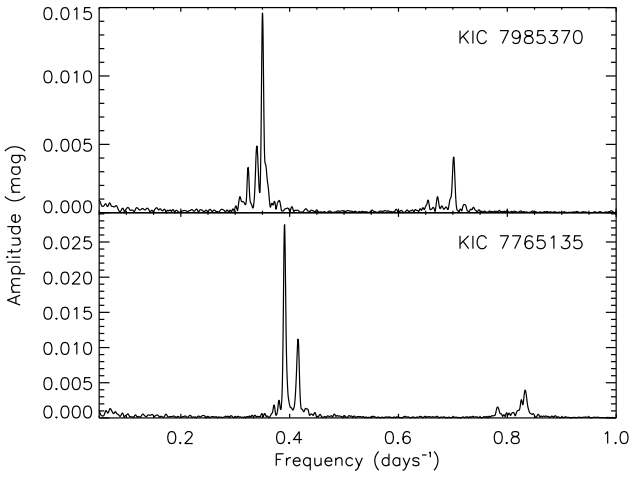

Fig. 7. Cleaned periodograms of the *Kepler* Q0+Q1+Q2+Q3 time series for KIC 7985370 (upper panel) and KIC 7765135 (lower panel).

model. With $v \sin i$, stellar radius R, and rotation period P known, the inclination of the rotation axis follows from

$$\sin i = \frac{(v \sin i) \cdot P}{2\pi R} \,. \tag{1}$$

In the absence of an accurate parallax value the stellar radius cannot be derived from the effective temperature and luminosity. If we adopt the radius for a ZAMS star with the effective temperature of our targets ($T_{\rm eff} = 5800\,$K), $R \approx 1.1\,R_\odot$, we get $\sin i = 0.967$ ($i = 75^\circ \pm 15^\circ$) for both stars. However, as stated in Sect. 3.3, the lithium content cannot provide a firm lower limit for the ages of these stars, which could also be as young as a few 10 Myr (post-T Tauri phase). Thus, allowing for such a young age, a $T_{\rm eff} = 5800\,$K is reached by a star of $1.5\,M_\odot$ at 10 Myr with a radius of about $2\,R_\odot$ according to the evolutionary tracks by Siess et al. (2000). In this case, an inclination of about 30° is deduced.

4.2. Bayesian photometric imaging

The method is basically that of Paper I. However, as the light curves are now significantly longer, the introduction of further free parameters was inevitable. The latitudinal dependence of rotation frequency $\Omega(\beta)$ (Eq. 2) now contains a $\sin^4\beta$-term and, more important, the prescription for spot area evolution is much more detailed. Furthermore, the likelihood function (Eq. 3) is generalized by taking into account an unknown linear trend in the data. To tackle the problem of strong correlations between some parameters, an essential new ingredient is the usage of an orthogonalized parameter space, where the steered random walk of the Markov chains is performed. For the sake of clarity, due to these new features, the basics of the method are explained in this section, although they can also found in Paper 1. A full account of the method must be deferred to a forthcoming paper (Fröhlich 2012).

A light-curve fitting that represents spots as dark and circular regions has the advantage of reducing the dimensionality of the problem and to promptly provide us with average parameters (area, flux contrast, position, etc.) for each photospheric active region. Of course, there are other techniques, which are based on different assumptions, to reconstruct surface features photometrically as the inversion of *Kepler* light curves done by, e. g., Brown et al. (2011).

Our aim is to present a low-dimensional spot model, with few spots only, that fits reasonably well the data regardless to very low-amplitude details that require a high degree of complexity. In a Bayesian context this claim could be even quantified. Ideally, one should estimate the so-called *evidence*, the integral over the posterior probability distribution. It would provide a measure of the probability of a n-spot model and, therefore, allow one to constrain the number of spots n that are really needed. For numerical reasons we are compelled to resort instead to the less demanding Bayesian Information Criterion (BIC) by Schwarz (1978). The latter or any other related criterion expresses Occam's razor in mathematical terms without the need to compute the evidence. Unfortunately, we have to admit that – due to the unprecedented accuracy of the *Kepler* data – we could not reach this goal with only seven or nine spots. There is obviously more information in the data than our most elaborate model is able to account for.

Dorren's (1987) analytical star-spot model, generalized to a quadratic limb-darkening law, was used. The two coefficients are taken from the tables of Claret & Bloemen (2011) for a microturbulence velocity of $\xi = 2\,\mathrm{km\,s^{-1}}$ and are used for both the unperturbed photosphere and the spots.

Four parameters describe the star as a whole: One is the cosine of the inclination angle i. Three parameters (A, B and C) describe the latitudinal dependence of the angular velocity. With β being the latitude value, the angular velocity Ω is parameterized by a series expansion using Legendre polynomials:

$$\begin{aligned}\Omega(\beta) = A \;&+\; 3B\left(5\sin^2\beta - 1\right)/2 + \\ &+\; C\left(315\sin^4\beta - 210\sin^2\beta + 15\right)/8\,. \end{aligned}\tag{2}$$

The equatorial angular velocity is $\Omega_{\rm eq} = A - 3B/2 + 15C/8$ and the equator-to-pole differential rotation $\mathrm{d}\Omega = 15B/2 + 105C/8$. In the case of the equator rotating faster than the poles $\mathrm{d}\Omega$ is negative. In what follows the minus sign is suppressed, and only the absolute value $|\mathrm{d}\Omega|$ is given. Both stars are definitely rotating like the Sun.

As in Paper 1, all star spots have the same intensity κ relative to the unspotted photosphere and are characterized by two position coordinates (latitude and initial longitude) and by their radius. All these are free parameters in the model. Other spot parameters are the rotation period, which defines the spot longitude at any time and is tied to the latitude via Eq. 2. The hemisphere, to which a spot belongs to, is to be found by trial and error. Further parameters describe the spot area evolution.

As our photometric analysis mainly aims at estimating the level of surface differential rotation, our focus is on *long-lived* spots. Longevity of star spots is at the heart of our approach. In order to obtain, in view of the extraordinary length of the time series, a satisfying fit, more freedom has been given to spot area evolution with respect to Paper 1. It is now parameterized by up to eight parameters.

Spot area is given in units of the star's cross-section. Area evolution is assumed to go basically linearly with time. The underlying physical reason is that then, at least in the case of a decaying spot, the slope of the area–time relation is somehow related to the turbulent magnetic diffusivity. With the aim of enhancing flexibility and to describe the waxing and waning of a spot, three consecutive slope values are considered. The time derivative of spot area is then a mere step function over time. Step height measures the increase/decrease of area per day. So,

there are six free parameters: three slope values, two dates of slope change, and the logarithm of spot area at some point of the time series. We have done even a little bit more. In order to prevent sharp bends in spot area evolution, some smoothing is introduced. Each date where the slope changes is replaced by a time interval within which the slope is linearly interpolated between the two adjacent values. This makes the second time derivative of spot area a mere step function of time, described by six parameters. To get the integrated area itself as function of time two constants of integration enter, thus bringing the number of free parameters to describe a spot's area evolution to a total of eight.

In addition to the free parameters of the model there are derived ones, the marginal distributions of which are of interest. An example is the rotational period. It follows from the longitudes of the spot centre at the beginning of the time series and at its end.

All parameters are estimated in a Bayesian manner, i. e. their mean values as well as the corresponding uncertainties follow straightforwardly from the data alone. To maintain a flat prior distribution in parameter space, all dimensional parameters like periods or spot radii must actually be described by their logarithms. Only then the posterior probability distribution for a period will be consistent with that of a frequency and likewise the posterior for a radius with that of an area, i. e. it does not matter whether one prefers periods to frequencies or radii to areas.

The likelihood function (Eq. 3) assumes that the measurement errors have a Gaussian distribution in the magnitude domain. This is justified as long as the signal-to-noise ratio does not vary with changing magnitude, as it is for our data that span a full variation range of less than 0.1 magnitudes. It has the invaluable advantage that the likelihood function can be analytically integrated over measurement error σ, offset c_0, and linear trend d_0. To perform the integration over σ one has to use Jeffreys' $1/\sigma$-prior (cf. Kass & Wassermann 1996). The resulting *mean* likelihood depends on spot-modelling parameters $p_1 \ldots p_M$ only. It takes into account all possible error values, offsets and linear trends. By multiplying it with the prior, assumed constant in parameter space, one gets the posterior density distribution. All interesting quantities, parameter averages and confidence intervals, are then obtained by marginalization.

With the N magnitude values d_i measured at times t_i, their standard deviations σ_i, the model magnitudes $f_0(t_i, p_1 \ldots p_M)$, offset c_0, and trend d_0, the likelihood function is given by

$$\Lambda\left(\sigma, c_0, d_0, p_1 \ldots p_M; d_i\right) =$$

$$\prod_{i=1}^{N} \frac{1}{\sqrt{2\pi}\sigma_i} \exp\left(-\frac{\left(d_i - f_0\left(t_i, p_{1\ldots M}\right) - c_0 - d_0 \cdot (t_i - t_0)\right)^2}{2\sigma_i^2}\right). \quad (3)$$

We set $\sigma_i = s_i \cdot \sigma$, with relative errors s_i being normalized according to $\sum_{i=1}^{N} 1/s_i^2 = N$.

Parameter estimation by sampling the parameter space has been done by the Markov chain Monte Carlo (MCMC) method (cf. Press et al. 2007).

Often parameter values are highly correlated. As MCMC performs best in an orthogonalized parameter space, all parameters have been converted by a principal component analysis using singular value decomposition (cf. Press et al. 2007). Each parameter in this abstract space is linearly dependent on all of the original parameters. The reconstruction of the original parameter values can be done exploiting a subspace of that orthogonalized parameter space. The dimension of that subspace, the number of degrees of freedom, proves lower by roughly one third or even more than the number of original parameters.

4.3. Results

4.3.1. KIC 7985370

We have identified eleven gaps longer than an hour and two additional small jumps in the light curve (Fig. 8). The data set was accordingly divided into 14 parts. Each part has been assigned its individual error level, off-set and, in Case B (i. e. non-rectified data), linear trend. Hence, the likelihood (Eq. 3) is the product of 14 independent contributions.

KIC 7985370's inclination value i is – to be honest – ill-defined by the spot model applied to the *Kepler* photometry. Indeed, with only six spots the MCMC results in very dark spots ($\kappa \approx 0$) at very low inclination ($i \approx 10°$). But even for these unrealistic solutions the equator-to-pole differential rotations was 0.18 rad d^{-1}. Only with seven spots and allowing for enough spot evolution we arrived at acceptable inclination values (Fig. 9) and spot intensities (Fig. 10). If the inclination is fixed to the spectroscopically derived value of $i = 75°$ the residuals are rather high, ±2.46 mmag, exceeding the residuals of our best solution (±2.14 mmag) by far. Nevertheless, details of the solution with fixed inclination are also included in Table 5, where the results are presented.

Improving the 7-spot solution by adding an eighth spot leads formally to a better fit. As the new spot proves to be ephemeral, lasting only six rotations, it neither constrains the differential rotation nor adds any significant insight (one can always get a better result by adding short-lived features).

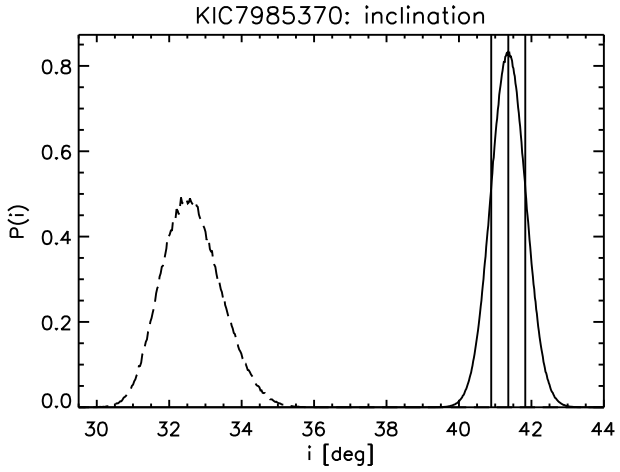

Fig. 9. Determination of the stellar inclination from *Kepler* photometry. Mean and 68-per-cent confidence region are marked by vertical lines (Case A only). Dashed: The corresponding marginal distribution for the original data with linear trends removed (Case B).

The marginal distributions of the seven spot frequencies (Case A only), combined into one plot, are shown in Fig. 11.

From the three parameters describing the star's surface rotation, A, B and C, the equatorial rotational period (Fig. 12) and the equator-to-pole differential rotation (Fig. 13) follow. The latter amounts to $0.1774^{+0.0004}_{-0.0005}$ rad d^{-1} (Case A) and 0.1729 ± 0.0002 rad d^{-1} (Case B), respectively. The difference is significant, considering the formal errors, albeit very small. In the case of fixed inclination ($i = 75°$) the differential rotation would be slightly enhanced, 0.1839 ± 0.0002 rad d^{-1}.

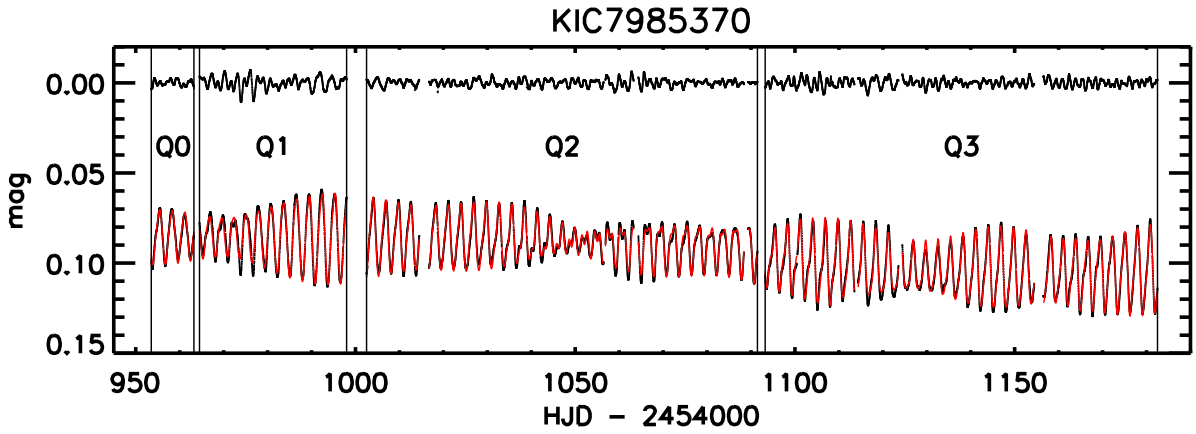

Fig. 8. *Kepler* light curve with best fit (solid red line, 2nd Case-A solution of Table 5) over-plotted. The residuals, shown at the top, are ±2.14 mmag. Obviously, the residuals are not homogeneous from one part of the light curve to another.

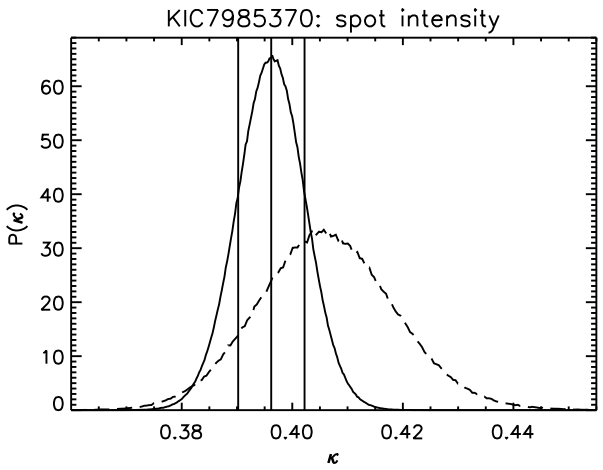

Fig. 10. Spot intensity related to the unspotted photosphere. Mean and 68-per-cent confidence region are marked by vertical lines (Case A only). Dashed: The corresponding marginal distribution for the original data with linear trends removed (Case B).

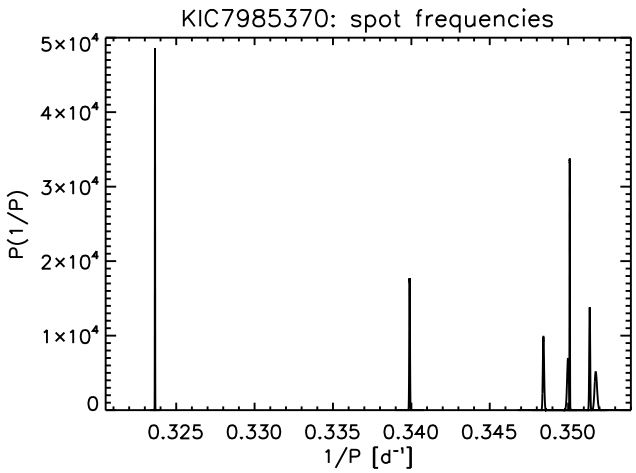

Fig. 11. All seven marginal distributions (Case A) of the spot frequencies. The three frequencies (0.324, 0.340, and 0.350 d^{-1}) seen in the low-resolution Fourier spectrum (Fig. 7) are confirmed by the results of our spot model.

The spot area evolution is depicted in Fig. 14. The sudden rise of spot # 7 seems to be an artefact. It falls into the gap between the end of Q2 data and the beginning of Q3 data. On the other hand, the sudden disappearance of spot # 3 is not related to any switching from one part of the light curve to the next one. The fall in area of spot # 1 at the end of the time series is somehow mirrored in an increase in the size of spot # 5. Maybe this indicates a flaw due to too much freedom in describing spot area evolution.

Expectation values with 1–σ confidence limits for various parameters are also quoted in Table 5.

One should be aware that there is more than one solution for each case. The second Case-A solution presented in Table 5 is the one that has the lowest residuals found so far. There is an other well-relaxed 7-spot solution with slightly larger residuals nearby in parameter space. In that solution the fastest spot (# 2), coming into existence near the end of the time series at JD~2455135, is located at a more southern latitude of −21°, resulting in a slightly increased differential rotation. All other spots are virtually unaffected. Further details of this second solution are given in Table 6.

Table 6. A second pair of 7-spot solutions for KIC 7985370.

parameter		Case A		Case B	
equ. period	P_{eq}	2.8202	±0.0002	2.8209	±0.0002
diff. rotation	dΩ	0.1943	±0.0002	0.1933	±0.0002
residuals		±2.20		±2.21	

Notes. The meaning of the entries is the same as in Table 5, i. e. periods are in days, the differential rotation in rad d^{-1}, and the residuals in mmag.

4.3.2. KIC 7765135

We have identified eleven gaps longer than an hour and three additional small jumps in the light curve (Fig. 15). The data set was accordingly divided into 15 parts. Each part has been assigned its individual error level, off-set and, in Case B (i. e. non-rectified data), linear trend. Hence, the likelihood function (Eq. 3) is the product of 15 independent contributions.

As the inclination is photometrically ill-defined, we fixed it to the spectroscopically derived value of $i = 75°$.

Table 5. Three 7-spot solutions for KIC 7985370. Listed are *expectation* values and 1-σ confidence limits.

parameter[a]			Case A[b]		Case A[b]		Case B[b]	
inclination		i	75.°0	*fixed*	41.°4	$^{+0.5}_{-0.5}$	32.°6	$^{+0.7}_{-0.9}$
1st	latitude	β_1	34.°0	$^{+0.1}_{-0.1}$	29.°4	$^{+0.4}_{-0.4}$	22.°6	$^{+0.5}_{-0.6}$
2nd	latitude	β_2	−10.°0	$^{+0.6}_{-0.9}$	−6.°9	$^{+0.9}_{-0.9}$	3.°3[c]	$^{+0.1}_{-0.1}$
3rd	latitude	β_3	32.°2	$^{+0.2}_{-0.2}$	29.°9	$^{+0.3}_{-0.3}$	27.°7	$^{+0.4}_{-0.4}$
4th	latitude	β_4	86.°8	$^{+0.1}_{-0.1}$	87.°5	$^{+0.1}_{-0.1}$	87.°8	$^{+0.1}_{-0.1}$
5th	latitude	β_5	53.°8	$^{+0.1}_{-0.1}$	53.°6	$^{+0.1}_{-0.1}$	51.°1	$^{+0.2}_{-0.2}$
6th	latitude	β_6	35.°8	$^{+0.2}_{-0.2}$	35.°8	$^{+0.3}_{-0.2}$	33.°0	$^{+0.3}_{-0.3}$
7th	latitude	β_7	29.°6	$^{+0.3}_{-0.2}$	19.°9	$^{+0.9}_{-0.9}$	10.°0	$^{+0.5}_{-0.6}$
1st	period	P_1	2.8581	$^{+0.0001}_{-0.0001}$	2.8563	$^{+0.0001}_{-0.0001}$	2.8572	$^{+0.0001}_{-0.0001}$
2nd	period	P_2	2.8350	$^{+0.0003}_{-0.0003}$	2.8428	$^{+0.0007}_{-0.0006}$	2.8475	$^{+0.0002}_{-0.0002}$
3rd	period	P_3	2.8541	$^{+0.0004}_{-0.0004}$	2.8572	$^{+0.0004}_{-0.0005}$	2.8644	$^{+0.0007}_{-0.0005}$
4th	period	P_4	3.0895	$^{+0.0001}_{-0.0001}$	3.0898	$^{+0.0001}_{-0.0001}$	3.0888	$^{+0.0001}_{-0.0001}$
5th	period	P_5	2.9382	$^{+0.0002}_{-0.0002}$	2.9421	$^{+0.0002}_{-0.0002}$	2.9417	$^{+0.0003}_{-0.0002}$
6th	period	P_6	2.8629	$^{+0.0003}_{-0.0004}$	2.8700	$^{+0.0004}_{-0.0003}$	2.8754	$^{+0.0005}_{-0.0004}$
7th	period	P_7	2.8490	$^{+0.0003}_{-0.0002}$	2.8460	$^{+0.0002}_{-0.0002}$	2.8487	$^{+0.0002}_{-0.0002}$
spot intensity		κ	0.437	$^{+0.005}_{-0.004}$	0.396	$^{+0.006}_{-0.006}$	0.406	$^{+0.012}_{-0.012}$
equ. period		$P_{\rm eq}$	2.8347	$^{+0.0003}_{-0.0003}$	2.8427	$^{+0.0007}_{-0.0006}$	2.8474	$^{+0.0003}_{-0.0002}$
deviation		C/B	0.28		0.28		0.21	
diff. rotation		dΩ	0.1839	$^{+0.0002}_{-0.0002}$	0.1774	$^{+0.0004}_{-0.0005}$	0.1729	$^{+0.0002}_{-0.0002}$
residuals			±2.46		±2.14		±2.12	

Notes. [(a)] Latitudes β are derived from the assumed law of differential rotation (Eq. 2). Periods P are given in days, the spot intensity κ is in units of the intensity of the unspotted surface. The ratio C/B measures the deviation from a pure $\sin^2$-law of differential rotation. The differential rotation dΩ (rad d^{-1}) is the equator-to-pole value of the shear. Residuals are in mmag. [(b)] Case A refers to rectified data, Case B to non-rectified one. In order to get the Case-B solution the Case-A solution has been taken as a starting point for the MCMC parameter estimation. In the first Case-A solution the inclination is fixed to $i = 75°$. [(c)] The second spot is near the equator, therefore, the hemisphere it belongs to is doubtful.

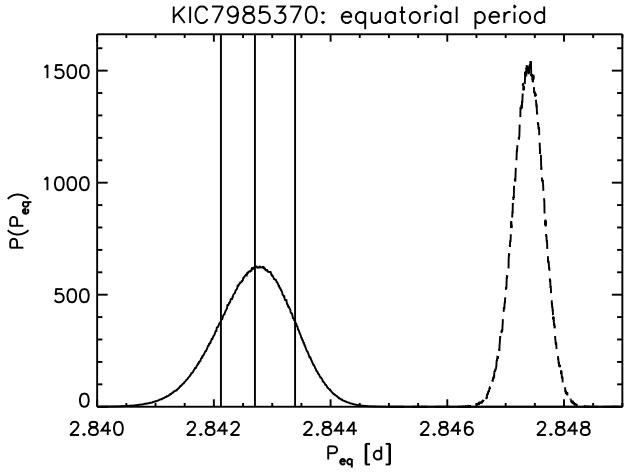

Fig. 12. Equatorial period of the star. Mean and 68-per-cent confidence region are marked by vertical lines (Case A only). Dashed: The corresponding marginal distribution for the original data with linear trends removed (Case B).

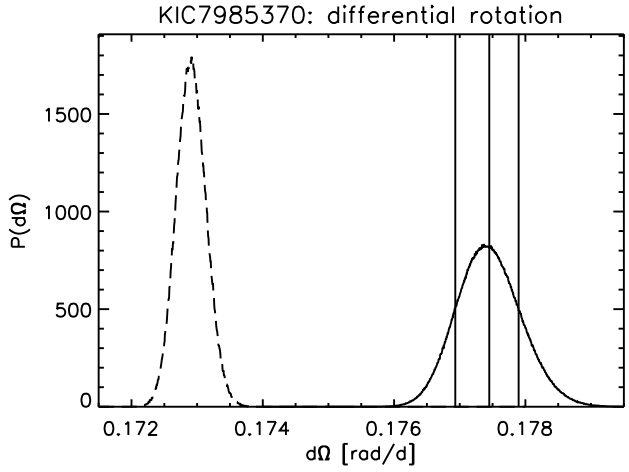

Fig. 13. Equator-to-pole differential rotation of the star. Mean and 68-per-cent confidence region are marked by vertical lines (Case A only). Dashed: The corresponding marginal distribution for the original data with linear trends removed (Case B).

Despite two spots more, the residuals, ±2.35 mmag, exceed those of the seven-spot model of KIC 7985370 (±2.14 mmag). This is not due to the fainter magnitude of KIC 7765135 compared to KIC 7985370, because the photometric uncertainties are typically 0.047 mmag for the former and 0.022 mmag for the latter. The reason may be that three of the nine spots are definitely short-lived with a life span as low as two months (cf. Fig. 20), which is less than twice the lapping time of 38 days between

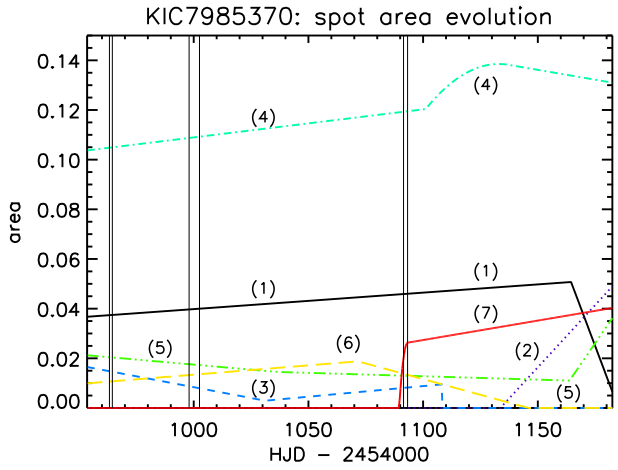

Fig. 14. Spot area evolution (Case A). Area is in units of the star's cross-section. Vertical lines mark the boundaries of the Q0 to Q3 quarters of data. A number in parenthesis indicates the spot number.

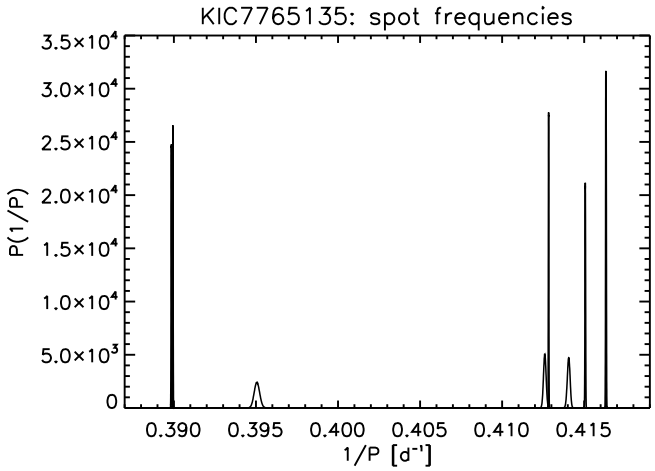

Fig. 17. Marginal distributions of the frequency for all the nine spots. The frequency values group around the two principal frequencies (0.391 and 0.414 d^{-1}) seen already in the Fourier spectrum (Fig. 7), which is the reason for the obvious "beating" phenomenon in Fig. 15 with a period of 40 days. The shortest and the longest frequency are a superposition of two frequencies.

the fastest and the slowest spot. We have to admit that dealing with nine spots goes already to the limit of the MCMC technique since the method's relaxation time becomes prohibitively long.

The marginal distribution of the spot rest intensity is shown in Fig. 16.

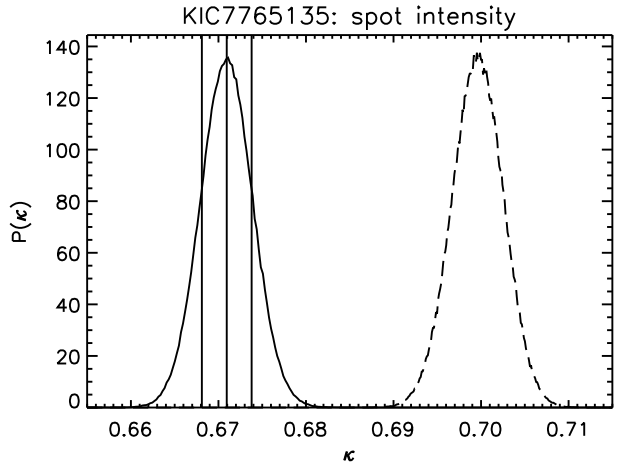

Fig. 16. Same as Fig. 10, for KIC 7765135.

The marginal distributions of the nine spot frequencies (Case A only), combined into one plot, are shown in Fig. 17.

From the three parameters describing the star's surface rotation, A, B and C, the equatorial rotational period (Fig. 18) and the equator-to-pole differential rotation (Fig. 19) follows. The latter amounts to 0.1760 ± 0.0003 rad d^{-1} (Case A) and $0.1774^{+0.0003}_{-0.0004}$ rad d^{-1} (Case B), respectively. As for KIC 7985370 the difference is small, but nevertheless significant.

The level of differential rotation does not depend on the number of spots considered. Neglecting the three short-lived spots, i.e. considering a six-spot model, would result in an equator-to-pole shear of 0.1777 ± 0.0006 rad d^{-1}.

Inclination does not significantly affect $d\Omega$. Indeed, decreasing the inclination from the adopted value of $i = 75°$ to 45° would result in a marginally larger differential rotation, three to four per cent. This is quite understandable. Inclination affects latitudes, but hardly periods.

A cursory glance cast at the beating pattern (Fig. 15) reveals a lapping time $P_{\rm beat} \sim 40$ days, which is nearly exactly the lapping time of 40.3 days from the two peaks of the cleaned periodogram (Fig. 7). From these 40.3 days one already gets an estimate of the minimum value for the differential rotation as $2\pi/P_{\rm beat} \sim 0.156$ rad d^{-1}, which is not far from that derived by the model.

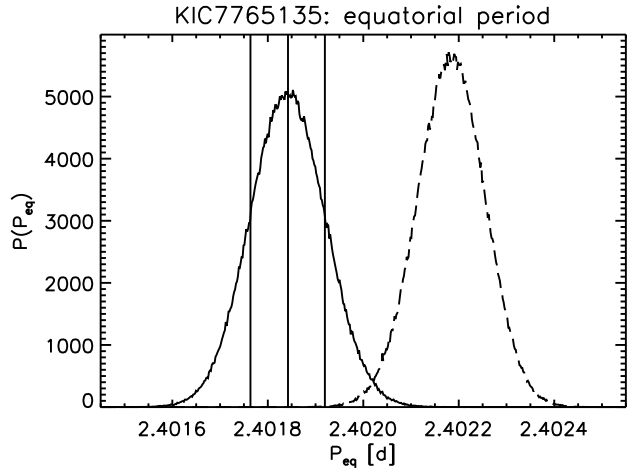

Fig. 18. Same as Fig. 12, for KIC 7765135.

The spot area evolution (Case A) is depicted in Fig. 20. The overwhelmingly large southern spot – at the beginning it fills to a large extent the southern hemisphere – may be an artefact. Because of its southern location its contribution to the light curve is rather modest. Perhaps it is actually a feature of the northern hemisphere, a non-circular extension of spot # 2. To prevent

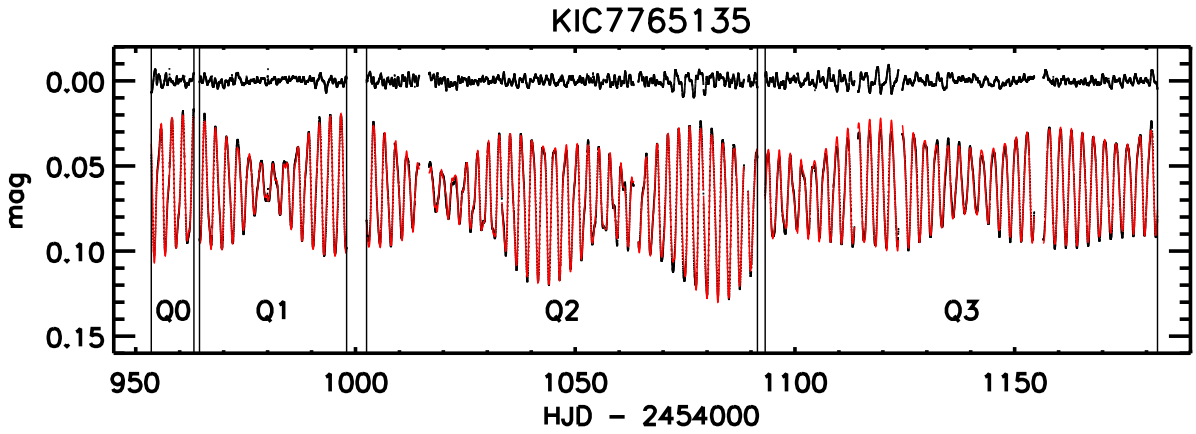

Fig. 15. *Kepler* light curve with best fit (solid red line, Case-A solution of Table 7) over-plotted. The residuals, shown at the top, are ±2.35 mmag. Obviously, the residuals are not homogeneous from one part of the light curve to another, hence, the stated ±2.35 mmag is to be considered an overall average.

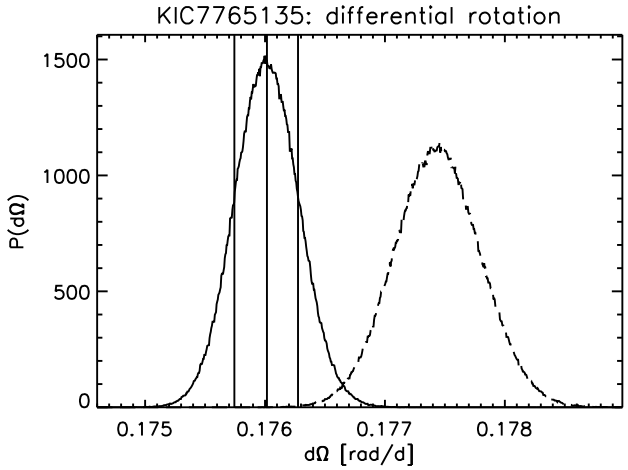

Fig. 19. Same as Fig. 13, for KIC 7765135.

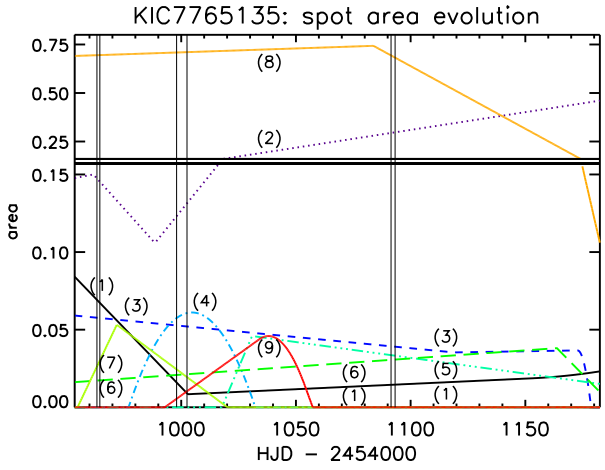

Fig. 20. Same as Fig. 14, for KIC 7765135. Three of the nine spots (# 4, # 7, and # 9) are short-lived ones. Note the change in scale in the upper part!

spot overlapping, spot # 8 had to be moved to the southern hemisphere. The reader should be aware that even in the case of a large spot the whole spot region has been assigned the angular velocity of its centre. Differential rotation is, to be exact, not compatible with a fixed circular shape. This is a shortcoming of our simple model.

In the case of KIC 7765135 it cannot be excluded that spot area evolution is partly driven by the need to avoid overlapping of spots.

Expectation values with 1–σ confidence limits for various parameters are compiled in Table 7.

5. Discussion

5.1. Chromospheric and coronal activity

With the aim of making a comparison with the chromospheric activity of stars similar to our targets, we considered eighteen stars in the Pleiades cluster, among those investigated by Soderblom et al. (1993b), that have an early-G spectral type or an effective temperature close to our targets and a $v \sin i$ between 4 and 18 km s^{-1}. With a spectral subtraction analysis they found values of the net Hα emission between 100 and 500 mÅ and surface fluxes ranging from 1.0×10^6 to 2.9×10^6 erg cm^{-2} s^{-1}.

The net emission filling the core of the Ca II-λ8542 line ranges from about 300 to 600 mÅ and the corresponding flux is in the range 1.0–2.7×10^6 erg cm^{-2} s^{-1}. The values of these activity indicators for our two targets are inside all these ranges, suggesting an activity level comparable to the Pleiades stars (age ∼ 130 Myr). The X-ray luminosity for these Pleiades members, as evaluated by Stauffer et al. (1994) and Marino et al. (2003), is in the range $\log L_X = 28.7$–29.7, which is just below the saturation threshold of $\log L_X = 30.0$ found by Pizzolato et al. (2003) for Sun-like stars. Moreover, according to the works of Pizzolato et al. (2003) and Soderblom et al. (1993b), the saturation would occur for rotation periods shorter than about 2.0 days. Another helpful work dealing with chromospheric activity in stars belonging to the young open clusters IC 2391 and IC 2602 (age ≈ 30 − 50 Myr) shows that the chromospheric flux measured in the core of Ca II–λ8542 line saturates at a value of $\log(R'_{8542}) = \log(F'_{8542}/\sigma T\mathrm{eff}^4) \approx -4.2$ (Marsden et al. 2009). A similar behaviour was already found for the Pleiades by Soderblom et al. (1993b). The $\log(R'_{8542})$ values of −4.5 and −4.6 that can be derived for KIC 7985370 and KIC 7765135, respectively, are lower than, but not very far from, this saturation level. From the ROSAT X-ray count and the distance quoted

Table 7. Two 9-spot solutions for KIC 7765135 with inclination being fixed to $i = 75°$. Listed are *expectation* values and 1-σ confidence limits.

parameter[a]			Case A[b]		Case B[b]	
inclination		i	75.°0	*fixed*	75.°0	*fixed*
1st	latitude	β_1	20.°4	$^{+0.1}_{-0.1}$	20.°0	$^{+0.1}_{-0.1}$
2nd	latitude	β_2	76.°3	$^{+0.2}_{-0.2}$	75.°1	$^{+0.2}_{-0.2}$
3rd	latitude	β_3	1.°9	$^{+0.2}_{-0.1}$	0.°8	$^{+0.2}_{-0.2}$
4th	latitude	β_4	21.°1	$^{+0.3}_{-0.3}$	20.°5	$^{+0.3}_{-0.3}$
5th	latitude	β_5	0.°9	$^{+0.3}_{-0.4}$	0.°7	$^{+0.3}_{-0.2}$
6th	latitude	β_6	12.°1	$^{+0.1}_{-0.1}$	11.°7	$^{+0.1}_{-0.1}$
7th	latitude	β_7	16.°3	$^{+0.3}_{-0.3}$	17.°2	$^{+0.3}_{-0.3}$
8th	latitude	β_8	−75.°9	$^{+0.2}_{-0.2}$	−74.°4	$^{+0.2}_{-0.2}$
9th	latitude	β_9	60.°2	$^{+0.4}_{-0.4}$	59.°4	$^{+0.4}_{-0.4}$
1st	period	P_1	2.4223	$^{+0.0001}_{-0.0001}$	2.4222	$^{+0.0001}_{-0.0001}$
2nd	period	P_2	2.5651	$^{+0.0001}_{-0.0001}$	2.5653	$^{+0.0001}_{-0.0001}$
3rd	period	P_3	2.4020	$^{+0.0001}_{-0.0001}$	2.4022	$^{+0.0001}_{-0.0001}$
4th	period	P_4	2.4237	$^{+0.0004}_{-0.0004}$	2.4231	$^{+0.0005}_{-0.0005}$
5th	period	P_5	2.4019	$^{+0.0001}_{-0.0001}$	2.4022	$^{+0.0001}_{-0.0001}$
6th	period	P_6	2.4092	$^{+0.0001}_{-0.0001}$	2.4092	$^{+0.0001}_{-0.0001}$
7th	period	P_7	2.4151	$^{+0.0004}_{-0.0005}$	2.4172	$^{+0.0005}_{-0.0005}$
8th	period	P_8	2.5645	$^{+0.0001}_{-0.0001}$	2.5641	$^{+0.0001}_{-0.0001}$
9th	period	P_9	2.5313	$^{+0.0010}_{-0.0010}$	2.5311	$^{+0.0009}_{-0.0009}$
spot intensity		κ	0.671	$^{+0.003}_{-0.003}$	0.700	$^{+0.003}_{-0.003}$
equ. period		$P_{\rm eq}$	2.4018	$^{+0.0001}_{-0.0001}$	2.4022	$^{+0.0001}_{-0.0001}$
deviation		C/B	−0.008		−0.008	
diff. rotation		dΩ	0.1760	$^{+0.0003}_{-0.0003}$	0.1774	$^{+0.0003}_{-0.0004}$
residuals			±2.35		±2.29	

Notes. [(a,b)] The meaning of the superscripts is the same as in Table 5.

in Table 2 we evaluated the X-ray luminosity of KIC 7985370 through the relation proposed by Fleming et al. (1995), $L_{\rm X} = 4\pi d^2(8.31 + 5.30\,HR1) \times 10^{-12}$ erg s^{-1}, where the hardness ratio is $HR1 = 0.23$ (Voges et al. 2000). The value of $\log L_{\rm X} = 29.68^{+0.15}_{-0.20}$ confirms the non-saturated regime for KIC 7985370.

5.2. General considerations on the spot model

Despite the fact that both stars are very active ones and exhibit filled-in absorption of several chromospheric activity indicators, our photometric analysis is in terms of dark surface features only. Allowing for bright ones too, would make the MCMC approach usually unstable. Anyway, photometry alone seems to be unable to discriminate even between dark and bright spots (e.g., Lüftinger et al. 2010).

As a comparison of the two cases A and B reveals, the results of our spot modelling are hardly influenced by the rectification procedure. The smaller residuals for non-rectified data (Case B) are very likely due to the fact that the Case-B likelihood function (Eq. 3) also takes into account a linear trend in the data, individually for each part of the light curve. This allows for more freedom in fitting the data and results in a slightly better fit.

The reader should be aware that the estimated parameter values and their often surprisingly small errors are those of the model constrained by the data. Error bars indicate the "elbow room" of the model, nothing more.

5.3. Frequencies

It is remarkable that the frequencies that stand out in the power spectrum of the light curves (Fig. 7) represent the distribution of spot frequencies (Figs. 11 and 17) astonishingly well. The lapping time, as a measure of the lower limit of surface differential rotation, follows already from the periodogram analysis! However, in order to get an estimate of the full equator-to-pole span of the latitudinal shear, including its sign, one needs latitudinal information.

5.4. Inclination

Combining the inclination value from photometry, $i \approx 40°$, with the spectroscopically measured projected rotational velocity $v \sin i$ (Table 2) allows us to determine in the case of KIC 7985370 the star's radius. Taking the shortest rotational period ($P_{\rm eq}$), one arrives at $R = 1.42$–$1.44 R_\odot$. This (minimal) radius is larger than the ZAMS value of $R \approx 1.1\,R_\odot$, but smaller than the $R \approx 2\,R_\odot$ for a star of $1.5 M_\odot$ at 10 Myr. Hence, the photometrically derived radius is within the expected range. As stated in Sect. 4.3.2, in the case of KIC 7765135 the photometric inclination is badly defined. Therefore, the inclination has been fixed to $i = 75°$, assuming the radius to have its ZAMS value.

5.5. Spot contrast and spot longevity

Although both stars share the same spectral type and age, there are differences concerning the spots. The spots of KIC 7985370 seem to be darker and longer living than those of KIC 7765135.

We would like to remind that a "spot" may be in fact a group of smaller spots that all together form an active region, which could also include bright features.

For KIC 7765135, the spot contrast, $\kappa \approx 0.7$, looks rather normal. It is similar to the previously studied case of KIC 8429280 (Paper I). The corresponding temperature contrast, the ratio between spot and photospheric temperature $T_{\rm sp}/T_{\rm ph}$, is 0.9, assuming that the "white light" *Kepler* flux matches the bolometric conditions. The much darker spots, $\kappa \approx 0.4$, in the case of KIC 7985370 defy a simple explanation. There is no need for exceptionally small (and therefore dark) spots to prevent spot overlap.

Apart from a few late F-type stars with low or moderate activity observed by CoRoT (Mosser et al. 2009) where spots seem to be short-lived, there is strong evidence that spots in very active stars like our targets have rather long lives compared to the star rotation. Active longitudes lasting for months or years have been observed in young stars (e.g., Collier Cameron 1995; Hatzes 1995; Barnes et al. 1998; Huber et al. 2009; Lanza et al. 2011) and in the evolved components of close binary systems, like II Peg (e.g. Rodonò et al. 2000; Lindborg et al. 2011). This does not exclude that individual unresolved spots, which are composing the active region, have shorter evolution times, but the photospheric active region seen as an entity endures for a very long time in such cases.

Unlike KIC 7985370, in the case of KIC 7765135 mid-latitude spots (30–50°) are missing. This is reminiscent of the spot distribution of two fast-rotating early G dwarfs, He 520 and He 699, of the α Persei cluster studied by Barnes et al. (1998). Despite the fact that there is a clear distinction between

near-equator and near-pole spots, with regard to spot lifetimes, no correlation seems to exist between lifetime and latitude, which is contrary to the case of the rapidly-rotating young AB Dor (Collier Cameron 1995), where only low- and intermediate-latitude spots are long-lived.

The sudden appearance of a full-grown spot at the beginning of a new quarter of data is suspicious and hints at an artefact (Fig. 14).

5.6. Differential rotation

Both stars exhibit low-latitude spots as well as high-latitude ones at the time of observation making them suitable for studying their latitudinal shear. The most robust and important result of the present work is the high degree of surface differential rotation found for both stars: $\mathrm{d}\Omega = 0.18\,\mathrm{rad\,d^{-1}}$. This exceeds threefold the solar value.

This estimate is rather robust, because any spot model with a few long-lasting spots able to reproduce the beating of the light curve must provide a value of equator-to-pole differential rotation that exceeds the lower limit of $2\pi/P_{\mathrm{beat}}$, irrespective of the number of spots used.

Inclination has a marginal effect since the periods found in the light curve do not depend on it.

We remark that the high value $\mathrm{d}\Omega$ relies on the assumption of spot longevity. It is always possible to get an excellent fit with many short-lived spots even for rigid rotation.

Very different values of differential rotation have been found for HD 171488 (V889 Her), a young (~50 Myr) Sun. For this star, which is rotating faster ($P = 1.33$ days) than our targets, a very high solar-type differential rotation $\mathrm{d}\Omega \approx 0.4$–$0.5\,\mathrm{rad\,d^{-1}}$, with the equator lapping the poles every 12–16 days, was found by both Marsden et al. (2006) and Jeffers & Donati (2008). Much weaker values ($\mathrm{d}\Omega \approx 0.04$) were derived instead for the same star by Järvinen et al. (2008) and Kővári et al. (2011). Huber et al. (2009) even claim their data being consistent with no differential rotation.

Marsden et al. (2011) report values of $\mathrm{d}\Omega$ in the range 0.08–$0.45\,\mathrm{rad\,d^{-1}}$ for a sample of stars similar to and slightly more massive than the Sun. Among these stars, HD 141943, a 1.3-$M_\odot$ star that is still in the PMS phase (age ~ 17 Myr), displays values of $\mathrm{d}\Omega$ ranging from about 0.23 to $0.44\,\mathrm{rad\,d^{-1}}$ in different epochs. A solar-type differential rotation, $\mathrm{d}\Omega \approx 0.2\,\mathrm{rad\,d^{-1}}$, was also found by Waite et al. (2011) for HD 106506, a G1 V-type star ($T_{\mathrm{eff}} = 5900$ K) that is very similar to our targets, but it is rotating faster ($P_{\mathrm{eq}} = 1.39$ days). Moreover, the Fourier transform technique applied to high-resolution spectra of a large sample of F- and early G-type stars indicates that differential rotation is rather frequently found (Reiners & Schmitt 2003; Reiners 2006). In their data, there is no clear dependency on the rotation period, but the strongest differential rotation, up to $\sim 1.0\,\mathrm{rad\,d^{-1}}$, occurs for periods between 2 and 3 days and values as high as $\sim 0.7\,\mathrm{rad\,d^{-1}}$ are encountered down to $P \sim 0.5$ days.

From ground-based photometry, which is basically devoted to cooler stars, a different behaviour, i.e. a differential rotation decreasing with the rotation period, seems to emerge (e.g., Messina & Guinan 2003). However, the precision of the ground-based light curves does not allow to draw firm conclusions and accurate photometry from space, as well as Doppler imaging, is needed for settling this point.

For mid-G to M dwarfs, weaker values of the latitudinal shears are generally found. In particular, Barnes et al. (2005) analyzed with the Doppler imaging technique a small sample of active stars in the spectral range G2–M2 finding a trend towards decreasing surface differential rotation with decreasing temperature. This suggests that the stellar mass must also play a significant role in this respect. The largest values for stars as cool as about 5000 K are $\mathrm{d}\Omega = 0.27\,\mathrm{rad\,d^{-1}}$ found by us in Paper I for KIC 8429280 (K2 V, $P = 1.16$ days) and $\mathrm{d}\Omega = 0.20\,\mathrm{rad\,d^{-1}}$ found by Donati et al. (2003) for LQ Hya (K2 V, $P = 1.60$ days). The slowly rotating ($P_{\mathrm{eq}} = 11.2$ d) and mildly active K2 V star ϵ Eri exhibits only little differential surface rotation ($0.017 \leq \mathrm{d}\Omega \leq 0.056\,\mathrm{rad\,d^{-1}}$) as a Bayesian reanalysis of the MOST light curve (Croll 2006; Croll et al. 2006) revealed (Fröhlich 2007).

Thus, there is an indication that a high differential rotation goes along with a high rotation rate.

The high differential rotation that we found for KIC 7985370 and KIC 7765135 disagrees with the hydrodynamical model of Küker et al. (2011), which instead predicts a rather low value of $\mathrm{d}\Omega \approx 0.08$ for an (evolved) solar-mass star rotating with a period as short as 1.3 days.

Surface differential rotation may even vary along the activity cycle. Indeed, certain mean-field dynamo models for rapidly rotating cool stars with deep convection zones predict torsional oscillations with variations of several percent in differential rotation (Covas et al. 2005). Of course, this cannot explain such extreme cases as LQ Hya where at times the surface rotation is solid body. According to Lanza (2006), to maintain the strong shear ($\sim 0.2\,\mathrm{rad\,d^{-1}}$) observed for LQ Hya in the year 2000 would imply a dissipated power exceeding the star's luminosity.

The differential rotation of rapidly-rotating solar-like stars has been recently investigated on theoretical grounds by Hotta & Yokoyama (2011). They found that differential rotation approaches the Taylor-Proudman state, i.e. the iso-rotation surfaces tend to become cylinders parallel to the rotation axis, when stellar rotation is faster than the solar one. In this case, the differential rotation is concentrated at relatively low latitudes with large stellar angular velocity. They show that the latitudinal shear (between the equator and latitude $\beta = 45°$) increases with the angular velocity, in line with our results and the recent literature.

6. Conclusions

In this paper, we have studied two Sun-like stars, KIC 7985370 and KIC 7765135, by means of high-resolution spectroscopy and high-precision *Kepler* photometry.

The high-resolution spectra allowed us to derive, for the first time, their spectral type, astrophysical parameters (T_{eff}, $\log g$, [Fe/H]), rotational and heliocentric radial velocities, and lithium abundance. All this information, combined with the analysis of the SED and proper motions, enabled us to infer their distance and kinematics, and to estimate the age of both stars in the range 100–200 Myr, although we cannot exclude that they could be as young as 50 Myr. Thus, these two sources should be already in the post-T Tauri phase.

As expected from their young age, both stars were found to be chromospherically active displaying filled-in Hα, Hβ, and Ca II IRT lines, as well as He I D_3 absorption. The surface chromospheric fluxes and the X-ray luminosity (for KIC 7985370), within the ranges found for stars with similar T_{eff} and $v \sin i$ in the Pleiades cluster, are just below the saturation level (Soderblom et al. 1993b). The flux ratio of two Ca II IRT lines and the Balmer decrement (for KIC 7765135 only) suggest that the chromospheric emission is mainly due to optically-thick surface regions analogous to solar plages.

We have applied a robust spot model, based on a Bayesian approach and a MCMC method, to the *Kepler* light curves

which span nearly 229 days and have an unprecedent precision ($\approx 10^{-5}$ mag). While seven long-lived spots were needed to perform a reasonable fit (at a 2-mmag level) of the light curve of KIC 7985370, we used up to nine spots in the case of KIC 7765135 due to a shorter lifetime of its spots. Because of the exceptional precision of the *Kepler* photometry it is impossible to reach the Bayesian noise floor defined by, e. g., the BIC (Schwarz 1978) without increasing significantly the degrees of freedom and, consequently, the non-uniqueness of the solution. Provided spots are indeed long-lived, the equator-to-pole value of the shear amounts for both stars to 0.18 rad d^{-1}. This is in contrast with the theoretical models of Küker et al. (2011) that predict a moderate solar-type differential rotation even for fast-rotating main-sequence stars, unless the convection zone is shallower than predicted by the stellar models. Our results are instead in line with the scenario proposed by other modelers of a differential rotation that increases with the angular velocity (Hotta & Yokoyama 2011) and that can be also subject to changes along the activity cycle (Covas et al. 2005; Lanza 2006).

Acknowledgements. We would like to thank the *Kepler* project and the team who created the MAST *Kepler* web site and search interfaces. We have also to thank an anonymous referee for helpful and constructive comments. This work has been partly supported by the Italian *Ministero dell'Istruzione, Università e Ricerca* (MIUR), which is gratefully acknowledged. JMŻ acknowledges the Polish Ministry grant no N N203 405139. DM and AK acknowledge the Universidad Complutense de Madrid (UCM), the Spanish Ministerio de Ciencia e Innovación (MCINN) under grants AYA2008-000695 and AYA2011-30147-C03-02, and the Comunidad de Madrid under PRICIT project S2009/ESP-1496 (AstroMadrid). This research made use of SIMBAD and VIZIER databases, operated at the CDS, Strasbourg, France. This publication makes use of data products from the Two Micron All Sky Survey, which is a joint project of the University of Massachusetts and the Infrared Processing and Analysis Center/California Institute of Technology, funded by the National Aeronautics and Space Administration and the National Science Foundation.

References

Andersen, J., Gustafson, B., & Lambert, D. L. 1984, A&A, 136, 65
Barnes, J. R., Collier Cameron, A., Unruh, Y. C., Donati, J.-F., & Hussain, G. A. J. 1998, MNRAS, 299, 904
Barnes, J. R., Collier Cameron, A., Donati, J.-F., et al. 2005, MNRAS, 357, L1
Barrado y Navascués, D., Stauffer, J. R., & Jayawardhana, R. 2004, ApJ, 614, 386
Bonanno, A., Elstner, D., Rüdiger, G., & Belvedere, G. 2002, A&A, 390, 673
Bonanno, A. 2012, Geophysical & Fluid Dynamics, in press
Borucki, W. J., Koch, D., Basri, G., et al. 2010, Sci 327, 977
Brown, A., Korhonen, H., Berdyugina, S., et al. 2011, AAS Meeting Abstracts #218, p. 205.02
Buzasi, D. L. 1989, Ph.D. Thesis, Pennsylvania State Univ.
Cardelli, J. A., Clayton, G. C., & Mathis, J. S. 1989, ApJ, 345, 245
Castelli, F., & Hubrig, S. 2004, A&A, 425, 263
Catanzaro, G., Frasca, A., Molenda-Żakowicz, J, & Marilli, E. 2010, A&A, 517, A3
Chester, M. M. 1991, Ph.D. Thesis, Pennsylvania State Univ.
Claret, A., & Bloemen, S. 2011, A&A, 529, 75
Collier Cameron, A. 1995, MNRAS, 275, 534
Covas, E., Moss, D., & Tavakol, R. 2005, A&A, 429, 657
Croll, B. 2006, PASP, 118, 1351
Croll, B., Walker, G. A. H., Kuschnig, R., et al. 2006, ApJ, 648, 607
Cutri, R. M., Skrutskie, M. F., van Dyk, S., et al. 2003, 2MASS All-Sky Catalog of Point Sources, University of Massachusetts and Infrared Processing and Analysis Center (IPAC/California Institute of Technology)
Dikpati, M., & Gilman, P. A. 2001, ApJ, 559, 428
Donati, J.-F., Collier Cameron, A., & Petit, P. 2003, MNRAS, 345, 1187
Dorren, J. D. 1987, ApJ, 320, 756
Eggen, O. J. 1984, ApJS, 55, 597
Eggen, O. J. 1989, PASP, 101, 366
Fleming, T. A., Molendi, S., Maccacaro, T., & Wolter, A. 1995, ApJS, 99, 701
Frasca, A., & Catalano, S. 1994, A&A, 284, 883
Frasca, A., Alcalá, J. M., Covino, E., et al. 2003, A&A, 405, 149
Frasca, A., Guillout, P., Marilli, E., et al. 2006, A&A, 454, 301
Frasca, A., Biazzo, K., Kővári, Zs., Marilli, E., & Çakırlı, Ö. 2010, A&A, 518, 48
Frasca, A., Fröhlich, H.-E., Bonanno, A., et al. 2011, A&A, 532, A81 (Paper I)
Fröhlich, H.-E. 2007, Astron. Nachr., 328, 1037
Fröhlich, H.-E. 2012, Astron. Nachr., in prep.
Glebocki, R., & Gnacinski, P. 2005, The Catalogue of Rotational Velocities of Stars, ESA, SP-560, 571
Gorlova, N., Rieke, G. H., Muzerolle, J., et al. 2006, ApJ, 649, 1028
Grevesse, N., Asplund, M., Sauval, A. J., & Scott, P. 2010, Ap&SS, 328, 179
Guillout, P., Klutsch, A., Frasca, A., et al. 2009, A&A, 504, 829
Hall, J. C., & Ramsey, L. W. 1992, AJ, 104, 1942
Hatzes, A.P. 1995, ApJ, 451, 784
Hauschildt, P. H., Allard, F., & Baron, E. 1999, ApJ, 512, 377
Høg, E., Fabricius, C., Makarov, V. V., et al. 2000, A&A, 355, L27
Hotta, H., & Yokoyama, T. 2011, ApJ, 740, 12
Huber, K. F., Wolter, U., Czesla, S., et al. 2009, A&A, 501, 715
Järvinen, S. P., Korhonen, H., Berdyugina, S. V., et al. 2008, A&A, 488, 1047
Jeffers, S. D., & Donati, J.-F. 2008, MNRAS, 390, 635
Jenkins, J. M., Caldwell, D. A., Chandrasekaran, H., et al. 2010, ApJ, 713, L120
Kass, R. E., & Wassermann, L. 1996, J. Am. Stat. Association, 91, 1343
Klutsch, A., Guillout, P., Frasca, A., et al. 2010, in Highlights of Spanish Astrophysics VI, Proceedings of the IX Scientific Meeting of the Spanish Astronomical Society, ed. M. R. Zapatero Osorio, J. Gorgas, J. Maíz Apellániz, J. R. Pardo, & A. Gil de Paz, p. 534
Klutsch, A., Freire Ferrero, R., Guillout, P., et al. 2012, in prep.
Koch, D. G., Borucki, W. J., Basri, G., et al. 2010, ApJ, 713, L79
Korhonen, H., & Elstner, D. 2011, A&A, 532, 106
Kővári, Zs., Frasca, A., Biazzo, K., et al. 2011, Proceedings IAU Symposium No. 273 "Physics of Sun and Star Spots", D. P. Choudhary & K. G. Strassmeier, eds., Cambridge Univ. Press, p. 121
Küker, M., Rüdiger, G., & Kitchatinov, L. L. 2011, A&A, 530, A48
Kurucz, R. L. 1993, A new opacity-sampling model atmosphere program for arbitrary abundances. in Peculiar versus normal phenomena in A-type and related stars, IAU Colloquium 138, ed. M. M. Dworetsky, F. Castelli, R. Faraggiana, A.S.P Conferences Series Vol. 44, p. 87
Kurucz, R. L., & Avrett, E. H. 1981, SAO Special Rep. 391
Kurucz, R. L., & Bell, B. 1995, Kurucz CD-ROM No. 23. Cambridge, Mass.: Smithsonian Astrophysical Observatory.
Landman, D. A., & Mongillo, M. 1979, ApJ, 230, 581
Lanza, A. F. 2006, MNRAS, 373, 819
Lanza, A. F., Rodonò, M., & Zappala, R. A. 1994, A&A, 290, 861
Lanza, A. F., Bonomo, A. S., Pagano, I., et al. 2011, A&A, 525, A14
Lindborg, M., Korpi, M. J., Hackman, T., et al. 2011, A&A, 526, A44
Lüftinger, T., Fröhlich, H.-E., Weiss, W. W., et al. 2010, A&A, 509, A43
Marino, A., Micela, G., Peres, G., & Sciortino, S. 2003, A&A, 406, 629
Marsden, S. C., Donati, J.-F., Semel, M., Petit, P., & Carter, B. D. 2006, MNRAS, 370, 468
Marsden, S. C., Carter, B. D., & Donati, J.-F. 2009, MNRAS, 399, 888
Marsden, S. C., Jardine, M. M., Ramírez Vélez, J. C., et al. 2011, MNRAS, 413, 1939
Martínez-Arnáiz, R., Maldonado, J., Montes, D., Eiroa, C., & Montesinos, B. 2010, A&A, 520, A79
Messina, S. & Guinan, E. F. 2003, A&A, 409, 1017
Mikolajewska, J., & Mikolajewski, M. 1980, Acta Astron., 30, 347
Montes, D., Fernández-Figueroa, M. J., De Castro, E., & Cornide, M. 1995, A&AS, 109, 135
Montes, D., López-Santiago, J., Gálvez, M. C., et al. 2001a, MNRAS, 328, 45
Montes, D., López-Santiago, J., Fernández-Figueroa, M. J., & Gálvez, M. C. 2001b, A&A, 379, 976
Mosser, B., Baudin, F., Lanza, A. F., et al. 2009, A&A, 506, 245
Nelson, N. J., Brown, B. P., Brun, S., Miesch, M. S., & Toomre, J. 2011, 217th AAS Meeting, #155.12, Bulletin of the American Astronomical Society, Vol. 43
Nordström, B., Mayor, M., Andersen, J., et al. 2004, A&A, 418, 989
Parker, E. N. 1955, ApJ, 122, 293
Pavlenko, Y. V., & Magazzù, A. 1996, A&A, 311, 961
Perryman, M. A. C., Lindegren, L., Kovalevsky, J., et al. 1997, A&A, 323, L49
Pfeiffer, M. J., Frank, C., Baumueller, D., et al. 1998, A&AS, 130, 381
Pigulski, A., Pojmański, G., Pilecki, B., & Szczygieł, D. M. 2009, Acta Astron., 59, 33
Pinsonneault, M. H., An, D., Molenda-Żakowicz, J., et al. 2012, ApJS, 199, 30
Pizzolato, N., Maggio, A., Micela, G., Sciortino, S., & Ventura, P. 2003, A&A, 397, 147
Press, W. H., Teulkolsky, S. A., Vetterling, W. T., & Flannery, B. P. 2007, Numerical Recipes, 3rd ed. (Cambridge Univ. Press, Cambridge)
Reiners, A. 2006, A&A, 446, 267
Reiners, A., & Schmitt, J. H. M. M. 2003, A&A, 398, 647
Roberts, D. H., Lehar, J., & Dreher, J. W. 1987, AJ, 93, 968

Rodonò, M., Messina, S., Lanza, A. F., Cutispoto, G., & Teriaca, L. 2000, A&A, 358, 624
Schwarz, G. 1978, The Annals of Statistics, 6, 461
Sestito, P., & Randich, S. 2005, A&A, 442, 615
Siess, L., Dufour, E., & Forestini, M. 2000, A&A, 358, 593
Soderblom, D. R., Jones, B. F., Balachandran, S., et al. 1993a, AJ, 106, 1059
Soderblom, D. R., Stauffer, J. R., Hudon, J. D., & Jones, B. F. 1993b, ApJS, 85, 315
Stauffer, J. R., Caillault J.-P., Gagne M., Prosser, C.F., & Hartmann, L. W. 1994, ApJS, 91, 625
Stauffer, J. R., Rebull, L. M., Carpenter, J., et al. 2005, AJ, 130, 1834
Steenbeck, M., Krause, F., & Rädler, K.-H. 1966, Z. Naturforsch. 21a, 369
Stetson, P. B. 2000, PASP, 112, 925
Udry, S., Mayor, M., & Queloz, D. 1999, Precise Stellar Radial Velocities, in IAU Colloq. 170, ed. J. B. Hearnshaw, & C. D. Scarfe, ASP Conf. Ser., 185, 367
Uytterhoeven, K., Moya, A., Grigahcène, A., et al. 2011, A&A, 534, A125
Voges, W., Aschenbach, B., Boller, T., et al. 1999, A&A, 349, 389
Voges, W., Aschenbach, B., Boller, T., et al. 2000, IAU Circ., 7432
Waite, I. A., Marsden, S. C., Carter, B. D., et al. 2011, MNRAS, 413, 1949